DOT/FAA/TC-23/48

Federal Aviation Administration
William J. Hughes Technical Center
Aviation Research Division
Atlantic City International Airport
New Jersey 08405

Development of Effective Taylor-Quinney Coefficient Tables of *MAT_224 for Aluminum 2024-T351, Titanium 6Al-4V, and Inconel 718 Alloys

July 2023

Final report

U.S. Department of Transportation
Federal Aviation Administration

NOTICE

This document is disseminated under the sponsorship of the U.S. Department of Transportation in the interest of information exchange. The U.S. Government assumes no liability for the contents or use thereof. The U.S. Government does not endorse products or manufacturers. Trade or manufacturers' names appear herein solely because they are considered essential to the objective of this report. The findings and conclusions in this report are those of the author(s) and do not necessarily represent the views of the funding agency. This document does not constitute FAA policy. Consult the FAA sponsoring organization listed on the Technical Documentation page as to its use.

This report is available at the Federal Aviation Administration William J. Hughes Technical Center's Full-Text Technical Reports page: actlibrary.tc.faa.gov in Adobe Acrobat portable document format (PDF).

Technical Report Documentation Page

Form DOT F 1700.7 (8-72) Reproduction of completed page authorized

1. Report No.	2. Government Accession No.	3. Recipient's Catalog No.
DOT/FAA/TC-23/48		

4. Title and Subtitle	5. Report Date
Development of Effective Taylor-Quinney Coefficient Tables of *MAT_224 for Aluminum 2024-T351, Titanium 6Al-4V, and Inconel 718 Alloys	July 2023
	6. Performing Organization Code

7. Author(s)	8. Performing Organization Report No.
Chung-Kyu Park, Kelly Carney, Paul Du Bois, and Cing-Dao Kan	

9. Performing Organization Name and Address	10. Work Unit No. (TRAIS)
George Mason University Center for Collision Safety and Analysis 4087 University Drive, Fairfax, VA 22030 USA	11. Contract or Grant No. 692M151840003

12. Sponsoring Agency Name and Address	13. Type of Report and Period Covered
U.S. Department of Transportation Federal Aviation Administration Air Traffic Organization Operations Planning Office of Aviation Research and Development Washington, DC 20591	Final Report
	14. Sponsoring Agency Code AIR-6A1

15. Supplementary Notes

The Federal Aviation Administration William J. Hughes Technical Center Aviation Research Division Technical Monitor was Daniel Cordasco.

16. Abstract

As a part of the FAA's Aircraft Catastrophic Failure Prevention Program (ACFPP), the LS-DYNA material model *MAT_224 was developed for computational modeling of high-speed impact problems, e.g., an actual turbine engine blade release event. Material impact imposes a temperature rise, which is estimated in *MAT_224 by the Taylor-Quinney Coefficient (TQC) that describes the percentage of plastic work converted into heat energy.

*MAT_224 input parameters for Aluminum 2024-T351, Titanium 6Al-4V, and Inconel 718 alloys were developed as part of the FAA's program. The three metallic materials showed good correlated ballistic impact simulations using inputs from a comprehensive series of test data and constant TQC parameters similar to the physical values referenced in literature. These constant physical TQCs are problematic for the impact analysis of a full engine installation and aircraft structure where the strain rates range from quasi-static to extremely high rates. The constant physical TQC does not adequately represent the material thermal softening process in low and intermediate-rate deformation properly, as it assumes adiabatic heating and neglects conduction. Therefore, effective TQCs values that compensate for the heat conduction at different strain rates are required for greater accuracy within *MAT_224.

In this research work, effective TQC tables for *MAT_224 were developed to replace current constant TQCs for those three metallic materials as referenced in literature. The methodology to create the effective TQC tables was developed, using a two-step approach. In Step 1, coupled thermal-structural analyses of tensile tests were conducted to verify the referenced constant TQC values and generate the temperature-strain curves at additional rates that were not covered by the physical tensile tests. In Step 2, structural-only analyses of tensile tests were conducted to calibrate and validate the effective TQC values at all the rates for the tables. The calibrated effective TQC tables can be incorporated into simulations for those three materials, and the methodology can be applied to create additional effective TQC tables for other metallic material.

17. Key Words	18. Distribution Statement
*MAT_224, LS-DYNA, impact, thermal softening, heat conduction, Taylor-Quinney Coefficient, TQC, plastic work, plastic heating, Aluminum 2024-T351, Titanium 6Al-4V, Inconel 718, coupled thermal-structural analysis	This document is available to the U.S. public through the National Technical Information Service (NTIS), Springfield, Virginia 22161. This document is also available from the Federal Aviation Administration William J. Hughes Technical Center at actlibrary.tc.faa.gov.

19. Security Classif. (of this report)	20. Security Classif. (of this page)	21. No. of Pages	22. Price
Unclassified	Unclassified	55	

Acknowledgements

The authors would like to express our gratitude to Dr. Jarrod Smith, Dr. Jeremy Seidt, and Prof. Amos Gilat at The Ohio State University, for sharing their insight and expertise along with the test data, photos, and videos generated during the tests. Their support greatly assisted with this research.

This research was conducted under FAA cooperative agreement 692M151840003 and sponsored by the Aircraft Catastrophic Failure Prevention Program (ACFPP).

Contents

1 Introduction 1

2 Material tensile tests 4

3 Thermal softening in *MAT_224 7

4 Methodology 9

4.1 Step 1: Thermal-structural coupled analysis 9

4.2 Step 2: Structural-only analysis 10

5 Finite element model and simulation 12

6 Effective TQC table creation 13

6.1 Al2024 14

6.2 Ti64 17

6.3 In718 20

6.4 Summary 23

7 Conclusions 26

8 References 27

A Al2024 tensile test simulation results in Step 1 ..... A-1

B Ti64 tensile test simulation results in Step 1 ..... B-1

C In718 tensile test simulation results in Step 1 ..... C-1

Figures

Figure 1. Geometry and dimensions of tensile test specimens of three materials (unit: mm) 4
Figure 2. Temperature change versus strain at local failure points of the specimen at various rates reproduced from Smith (2019). 5
Figure 3. TQC versus plastic strain at local failure areas of the specimen at various rates reproduced from Smith (2019). 6
Figure 4. Temperature vs strain curves of Al2024 at SR2 obtained from the first and second steps 11
Figure 5. FE model of the tensile test specimen 12
Figure 6. Temperature curves of a Al2024 specimen in the thermal-structural coupled analysis at SR1 13
Figure 7. Additional temperature vs. strain curves of Al2024 15
Figure 8. Calibrated effective TQC table of Al2024 16
Figure 9. Comparison of temperature vs. strain curves between thermal-structural coupled analysis (step 1) and structural-only analysis (step 2) on Al2024 16
Figure 10. Additional temperature vs. strain curves of Ti64 18
Figure 11. Calibrated effective TQC table of Ti64 19
Figure 12. Comparison of temperature vs. strain curves between thermal-structural coupled analysis (step 1) and structural-only analysis (step 2) for Ti64 19
Figure 13. Additional temperature vs. strain curves of In718 21
Figure 14. Calibrated effective TQC table of In718 22
Figure 15. Comparison of temperature vs. strain curves between thermal-structural coupled analysis (step 1) and structural-only analysis (step 2) on In718 22
Figure 16. Summary of TQCs for Al2024, Ti64, and In718 24

Tables

Table 1. Measured effective TQCs at various rates 4
Table 2. Thermal properties of Al2024, Ti64, and In718 8
Table 3. Summary of Al2024 simulations 15
Table 4. Summary of Ti64 simulations 18
Table 5. Summary of In718 simulations 21
Table 6. Summary of logistic function parameters 23

Acronyms

Acronym	Definition
ACFPP	Aircraft Catastrophic Failure Prevention Program
Al2024	Aluminum 2024-T351 alloy
DIC	Digital Image Correlation
FE	Finite Element
FAA	Federal Aviation Administration
GMU	George Mason University
GWU	George Washington University
In718	Inconel 718 alloy
NASA-GRC	National Aeronautics and Space Administration - Glenn Research Center
OSU	Ohio State University
Ti64	Titanium 6Al-4V alloy
TQC	Taylor-Quinney Coefficient

Executive summary

Failure of high-energy rotating turbine engine parts such as blades and rotors pose a leading risk to aviation safety. These violent events can hurl multiple fragments with varying size, speed, and damage potential. Engine and aircraft structures can be hit directly by the debris and experience significant stress from both the transmitted displacement wave from the fragment impacts as well as from the resulting rotor unbalance. The affected parts can experience a wide range of strain rates as they are subjected to large deformations, resulting in local plastic heating of the metallic structures involved. Properly accounting for the temperature rise and associated thermal softening is crucial for accurate prediction of penetration resistance and damage for metallic aircraft materials.

As a part of the FAA's Aircraft Catastrophic Failure Prevention Program (ACFPP), the LS-DYNA material model *MAT_224 was developed for computational modeling of high-speed impact problems, e.g., an actual turbine engine blade release event. Thermal softening in *MAT_224 uses a function to calculate the temperature increase induced by plastic work. The temperature rise in *MAT_224 is estimated by the Taylor-Quinney Coefficient (TQC), which describes the percentage of plastic work converted into heat energy. Typical *MAT_224 calculations assume metallic materials would be deformed under adiabatic conditions in such high-speed impact problems, and disregard or ignore the heat conduction effect.

As part of an FAA sponsored program, *MAT_224 input parameters for Aluminum 2024-T351, Titanium 6Al-4V, and Inconel 718 alloys have been developed using data from a comprehensive series of tests. Simulations using the three metallic material models using constant TQC parameters corresponding to the physical values referenced in literature showed good comparisons to ballistic impact tests simulating containment events. However, these constant physical TQCs in the current *MAT_224 material models are problematic in simulations of a full engine with unbalance resulting from blade loss. Both in full engine and longer duration event simulations, the strain rates range from quasi-static to extremely high rates. As a result, the constant physical TQC cannot properly represent the reduced material thermal softening process caused by heat conduction in low and intermediate-rate deformation. Effective TQC tables that consider heat conduction at different strain rates are required.

In this research work, effective TQC tables for *MAT_224 applicable to Aluminum 2024-T351, Titanium 6Al-4V, and Inconel 718 alloys were developed to replace the current constant TQCs. A methodology was developed that uses a two-step approach to develop and validate the effective TQC tables. In Step 1, coupled thermal-structural analyses of tensile tests were conducted to verify the referenced TQC values and generate the temperature-strain curves at

additional rates that were not covered by the physical tensile tests. In Step 2, structural-only analyses of tensile tests were conducted both to calibrate and validate the effective TQC values at all the rates for the effective TQC table. The calibrated effective TQC tables are able to be integrated into the *MAT_224 material model in LS-DYNA, and the methodology can be replicated to develop additional effective TQC tables for other metallic materials.

1 Introduction

A team consisting of George Mason University (GMU), The Ohio State University (OSU), George Washington University (GWU), the National Aeronautics and Space Administration - Glenn Research Center (NASA-GRC), and the Federal Aviation Administration (FAA) - Aircraft Catastrophic Failure Prevention Program (ACFPP) collaborated to develop a new constitutive material model in LS-DYNA for metallic materials. The research was directed toward improving the numerical modeling of turbine engine blade-out containment tests required for the certification of aircraft engines (Emmerling, Altobelli, Carney, & Pereira, 2014). This effort resulted in the development of the LS-DYNA constitutive material model *MAT_TABULATED_ JOHNSON_COOK, or simply *MAT_224 (Buyuk, 2014) (LSTC, 2017), for use in the LS-DYNA commercial finite element solver.

*MAT_224 is a general elasto-thermo-visco-plastic material model that utilizes a tabulated approach to incorporate arbitrary stress versus strain curves to define material plasticity, including arbitrary strain rate and temperature dependency. In a metallic blade impact event, adiabatic heating due to plastic work will cause temperatures to increase and the material to soften. In *MAT_224, rupture is modeled by an element erosion criterion using plastic strain, which can be defined as a function of the state of stress, strain rate, temperature, and element size.

As an extension of these efforts, *MAT_224 input parameters for three metal alloys, Aluminum 2024-T351 (Al2024), Titanium 6Al-4V (Ti64), and Inconel 718 (In718), have also been developed and released publicly (LS-DYNA Aerospace Working Group, 2023). The *MAT_224-Al2024 dataset (Version 2.2) was developed (Park C. K., Carney, Du Bois, Cordasco, & Kan, 2020) (Seidt, 2014) (Seidt, et al., 2022) (Seidt, Smith, Spulak, Lowe, & Gilat, 2022) and validated intensively with several ballistic impact simulation series.

1. Ballistic impact simulations of a sphere projectile to square Al2024 plates with various thicknesses (Park C. K., Carney, Du Bois, Cordasco, & Kan, 2020) (Kelley & Johnson, 2006)
2. Ballistic impact simulations of a cylindrical projectile onto circular Al2024 plates with various thicknesses (Park C. K., Carney, Du Bois, Cordasco, & Kan, 2020) (Pereira, Revilock, Lerch, & Ruggeri, 2013)
3. Ballistic impact simulations of 1/8-inch thick Al2024 plates with rectangular projectiles, having varying oblique incidence and attitude angles (Park, et al., 2020) (Pereira, Revilock, Lerch, & Ruggeri, 2013)

4. Ballistic impact simulations on large flat Al2024 panels with a blade-shaped Ti64 projectile designed to represent key aspects of a real turbine engine fan-blade release event (Park C. , Carney, Du Bois, Kan, & Cordasco, 2021).

The *MAT_224-Ti64 dataset (Version 1.3) was developed (Haight, Wang, Du Bois, Carney, & Kan, 2016) (Hammer, 2014) and validated with dynamic punch tests (Haight, Wang, Du Bois, Carney, & Kan, 2016) (Hammer, 2014) and ballistic tests of cylindrical projectiles impacting circular 1/2-inch thick Ti64 plates (Haight, Wang, Du Bois, Carney, & Kan, 2016) (Pereira, Revilock, Lerch, & Ruggeri, 2013). The *MAT_224-In718 dataset (Version 1.1 and 1.2) was developed (Dolci, Carney, Wang, Du Bois, & Kan, 2023 expected), and validated with ballistic tests of cylindrical projectiles impacting circular 1/2-inch thick In718 plates (Dolci, Carney, Wang, Du Bois, & Kan, 2023 expected) (Pereira, Revilock, Lerch, & Ruggeri, 2013) (Dolci, 2022). Overall, the ballistic impact simulations using the *MAT_224 material models of these three metals showed good correlations to the lab tests for a broad range of test conditions.

The thermal softening of metallic materials occurs when there is heat induced from the plastic deformation of the material, resulting in a stiffness reduction caused by the temperature rise. The thermal softening is dependent on the temperature field governed by heat generation and dissipation over the period of plastic deformation that occurs in the material. Although in general the heat dissipation includes the combined effects of conduction, convection, and radiation, here conduction is the dominant mechanism. When the plastic deformation rate of the material is high enough to neglect the heat conduction in the material, thermal softening occurs in an adiabatic condition. Conversely, if the plastic deformation happens in a quasi-static condition, it becomes an isothermal process, the material's temperature remains nearly constant, and there is little or no thermal softening. Originally, the *MAT_224 constitutive model was developed for the analysis of high-speed impact problems occurring on a short timescale, e.g., determining whether an engine containment case is breached by impact of a fan blade fragment. In such high-speed impact problems, it is assumed that a metallic material is deformed under an adiabatic condition. The *MAT_224 constitutive model implemented a function to calculate the temperature increase induced by plastic work, and its utilization ignored all heat dissipation.

In *MAT_224 the temperature rise is estimated using the Taylor-Quinney Coefficient (TQC), symbolically Beta (β), which describes the percentage of plastic work converted into heat energy. The physical TQC constants of metallic materials obtained from references (Ravichandran, Rosakis, Hodowany, & Rosakis, 2002) were adopted in the development of the *MAT_224 datasets of Al2024, Ti64, and In718. The TQC constants from the literature were checked, and in several cases, slightly adjusted during calibration of the models to specimen test

data. The *MAT_224 material models of the three metals, with the constant physical TQCs, produced correlated simulations in good agreement to both to high-rate mechanical property tests, and ballistic impact tests. However, these constant physical TQCs in the current material models of *MAT_224 could be problematic for the impact analysis of a full engine structure where the strain rates range from quasi-static to extremely high rates near the impact. The constant physical TQCs could also be problematic for longer duration analysis where the strain rates decrease after the extremely high rates from the initial impact. Depending on the rates of material deformation, the thermal softening of material transits from an isothermal process at a quasi-static rate to an adiabatic process at a high rate, which is distinguished by how much heat is conducted in the thermal softening process. Thus, the constant physical TQC cannot represent the material thermal softening process in low and intermediate-rate deformation properly due to lack of consideration for heat conduction. Effective TQCs that consider heat conduction at different rates are required to accurately simulate dynamic processes which involve plastic deformation over a broad range of strain rates.

Material tensile tests of Al2024, Ti64, and In718 have been conducted with full-field measurement systems to obtain effective TQC values at various strain rates (Smith, 2019). Measurement-derived effective TQC values of these three materials were calculated based on the temperature increase measured at the local failure area of the specimens. The effective TQC values were calculated at the various strain rates of the physical tensile tests. The effective TQC values measured from the temperature and strain field evolution observed in the experiments include the combined effects of heat generation from plastic deformation determined by the physical TQC, and the dissipation by heat conduction. The measured effective TQC can then be defined as a function (table) of the effective TQC values with respect to strain rates. However, this measured effective TQC table cannot be used as a direct input to *MAT_224 due to fundamental differences in temperature gradients. The *MAT_224 constitutive model has an absence of the heat conduction term, therefore the measured effective TQC table needs to be calibrated by the numerical analysis procedure described herein to develop the calibrated effective TQC table for *MAT_224. The calibrated TQC values at low and intermediate strain rates describe temperature rise at each rate associated with both heat generation and conduction.

In this research, the method to calibrate the effective TQC values at different rates was developed through two-step numerical analyses, and the calibrated effective TQC tables of Al2024, Ti64, and In718 were obtained and validated.

2 Material tensile tests

Material tensile tests of Al2024, Ti64, and In718 at six different strain rates at room temperature were conducted by The Ohio State University (OSU) (Smith, 2019). In these tests, the full-field strain and temperature were measured simultaneously to obtain temperature increase versus strain history and measure the effective TQCs at each rate. In this section, the test results are briefly summarized.

Figure 1 shows the geometry and dimensions of tensile test specimens of three materials, Al2024, Ti64, and In718. All specimens were fabricated from 0.5-inch hot rolled plates of three materials.

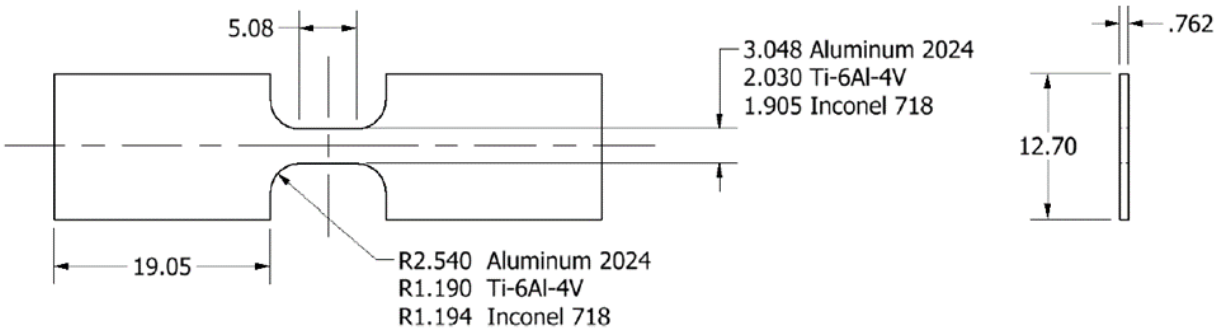

Figure 1. Geometry and dimensions of tensile test specimens of three materials (unit: mm)

Table 1 lists the measured effective TQCs measured at 6 nominal strain rates of tensile tests, from quasi-static (SR1) to high (SR6) rates.

Table 1. Measured effective TQCs at various rates

Nominal strain rate (s^{-1})		**Measured effective TQCs**		
		Al2024	**Ti64**	**In718**
SR1	0.0001	0.0	0.0	0.0
SR2	0.1	0.114	0.396	0.406
SR3	1.0	0.331	0.621	0.661
SR4	500	0.533	0.675	0.686
SR5	2,000	0.526	0.659	0.646
SR6	6,000	0.485	0.784	0.651

Figure 2 shows the curves of measured temperature change versus strain at the local failure point of the specimen at different strain rates (Smith, 2019). There was negligible temperature change at the quasi-static rate (10^{-4} /sec) in all three materials, which means that the thermal softening was in the isothermal condition. When the rate became higher, such as over 500 /sec in Al2024

and Ti64 and over 1.0 /sec in In718, the temperature increased linearly with strain; the thermal softening was in the adiabatic condition. It is observed that, at the rate of 0.1 sec in all three materials, the temperature increases with decreasing slope due to heat conduction.

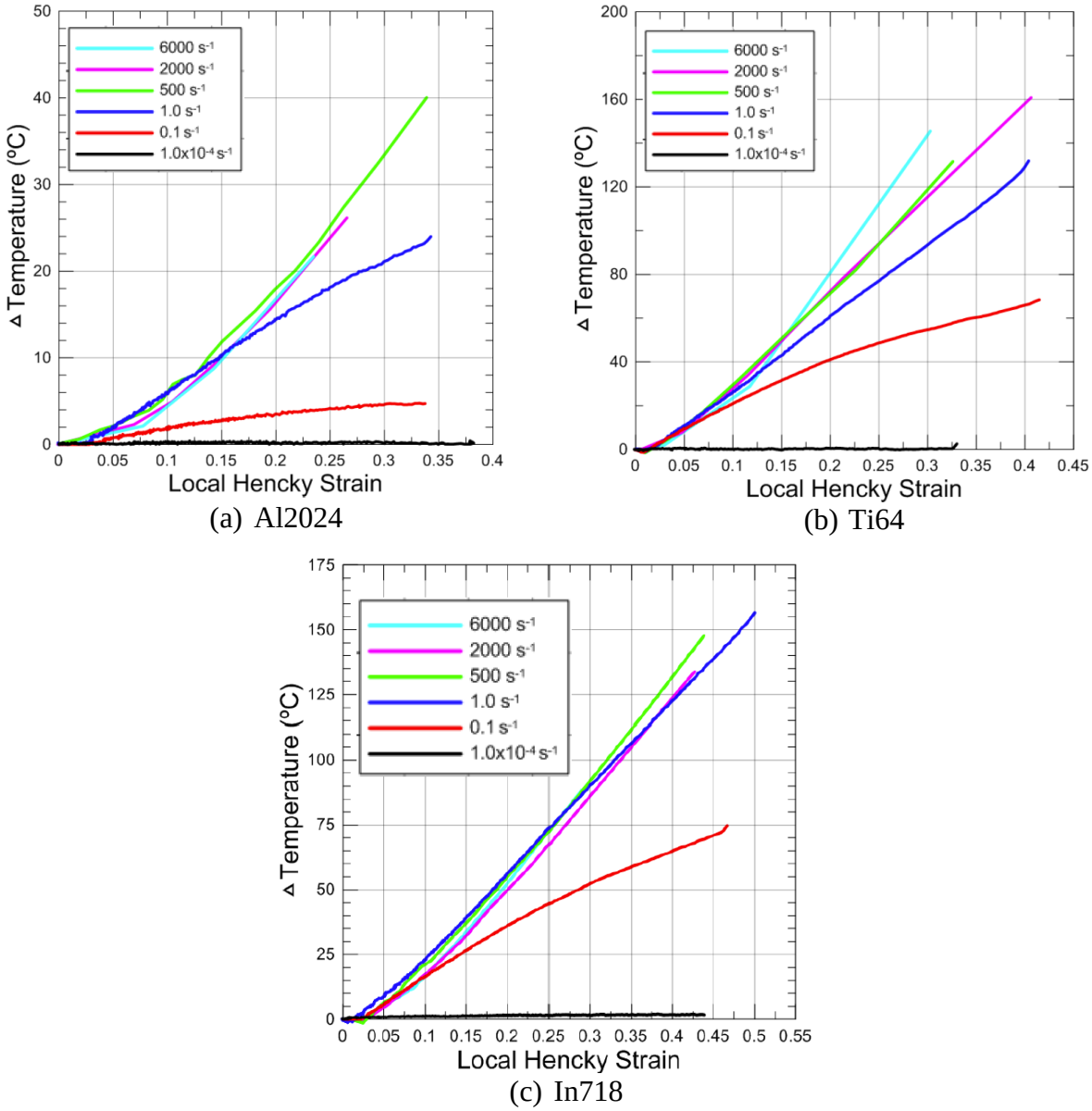

(a) Al2024 (b) Ti64

(c) In718

Figure 2. Temperature change versus strain at local failure points of the specimen at various rates reproduced from Smith (2019)

Figure 3 shows the curves of TQC versus plastic strain at various strain rates for the three materials (Smith, 2019). The TQC values were measured and averaged over the local failure area of the specimen. In the quasi-static rate (10^{-4} /sec), the TQC is zero because there is no temperature change, as shown in Figure 2. When the rate in the test is higher and the plastic

strain increases, the TQC value converges with the physical TQC value of each material. In the low rates, the TQC value becomes lower than the physical TQC value due to heat conduction, which is called the effective TQC value. The measured effective TQC values at each rate were obtained by averaging the TQC curves in Figure 3. The measured effective TQC tables for the three materials from the tensile tests are summarized in Table 1.

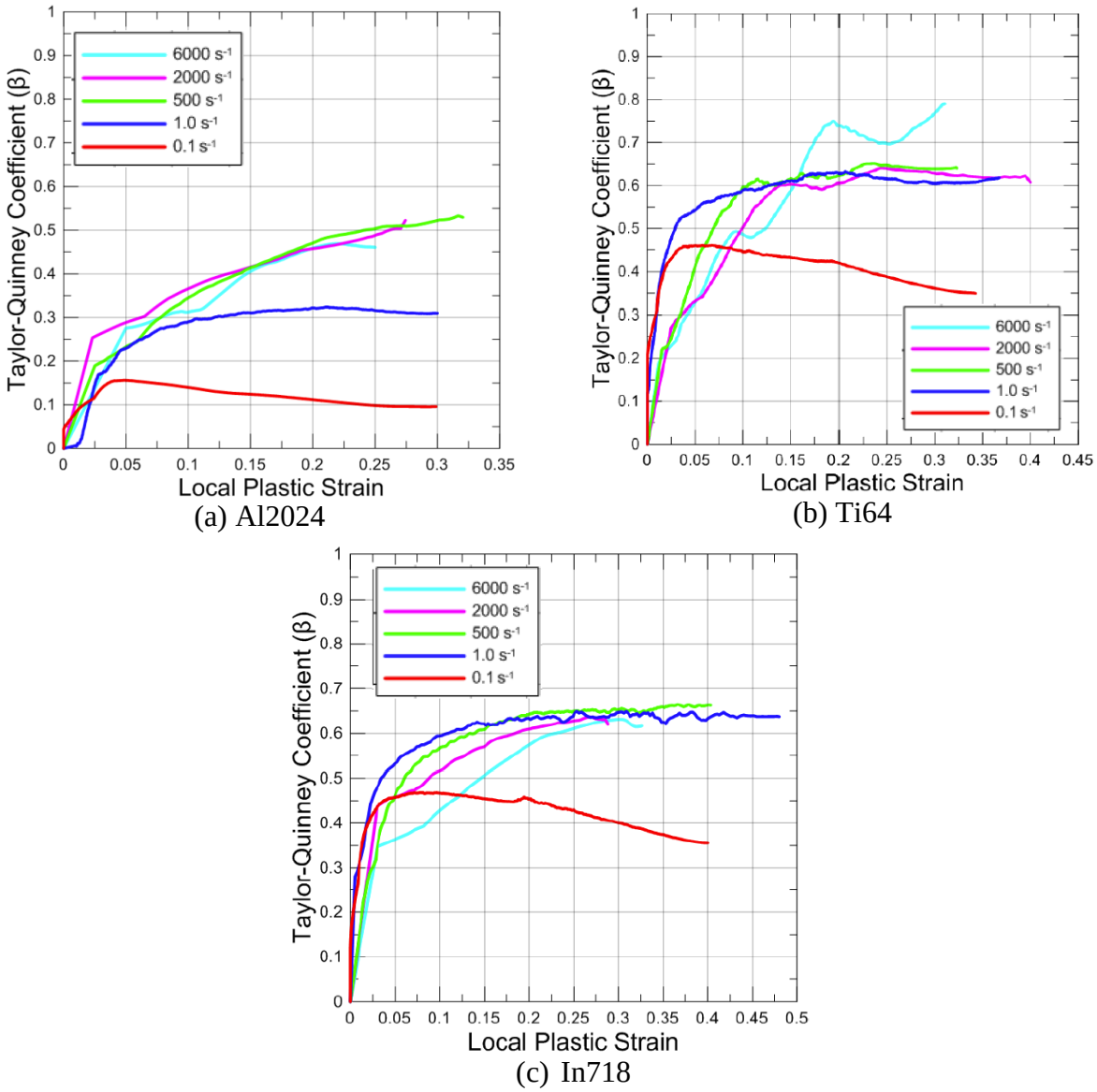

Figure 3. TQC versus plastic strain at local failure areas of the specimen at various rates reproduced from Smith (2019)

3 Thermal softening in *MAT_224

In general, the thermal softening of metallic materials is the result of a stiffness reduction caused by heat generated by impact and the associated temperature rise induced by plastic deformation of the material. Basically, thermal softening is dependent on heat generation and conduction over the period of plastic deformation that happens in the material. This is governed by the heat equation, as expressed in Equation 1.

$$\frac{\partial T(\mathbf{x},t)}{\partial t} = \frac{1}{\rho c_p}\left\{\nabla \cdot \left(k \cdot \nabla\left(T(\mathbf{x},t)\right)\right) + \dot{q}\right\} \quad 1$$

where ρ is the density, c_p is the heat capacity, k is the heat conductivity, T is the temperature, and $\dot{q}$ is the rate of the internal heat sources per unit volume. The internal heat sources of solid bodies can be described as heat generation by plastic work and defined in Equation 2, where β is the TQC, σ_y is the flow stress, and $\dot{\varepsilon}_p$ is the rate of the plastic strain.

$$\dot{q} = \beta \sigma_y \dot{\varepsilon}_p \quad 2$$

The TQC describes the percentage of plastic work converted into heat energy. So, Equation 1 means that the temperature change in the material over time results from heat conduction to and from surrounding material, which is the first term of the right side of Equation 1; and the heat generation induced by plastic deformation, which is the second term of the right side of Equation 1.

Originally, the *MAT_224 constitutive material model was developed for the analysis of high-velocity impact problems, where the thermal softening occurs in an adiabatic condition. So, in *MAT_224, the temperature change is set so that only heat generation as a result of plastic work is calculated and heat conduction is ignored, which is implemented in Equation 3.

$$\Delta T = \frac{1}{\rho c_p}\int \dot{q}\, dt = \frac{1}{\rho c_p}\int \beta\, \sigma_y \dot{\varepsilon}_p dt \quad 3$$

Initially, the TQC was defined as a constant in *MAT_224 and later the TQC was updated to be defined as a function of strain rate, temperature, plastic strain, and the state of stress.

The *MAT_224 input datasets for Al2024, Ti64, and In718 have been developed starting with the constant physical TQC of each material (Ravichandran, Rosakis, Hodowany, & Rosakis,

2002), shown in Table 2. With a constant physical TQC, the temperature change of a material is dependent only on the plastic work, which is a function of plastic strain and independent of the strain rate. As a result, the current *MAT_224 datasets for the three materials do not correctly represent the thermal softening of materials deforming at low and intermediate strain rates. To overcome this limitation, the TQC value can be adjusted according to the strain rates, which becomes the effective TQC table.

Table 2. Thermal properties of Al2024, Ti64, and In718

	Referenced physical TQC (β)	**Density (ρ)** kg / m^3	**Heat capacity (c_p)** $J / kg\ ^oC$	**Heat conductivity (k)** $W / m\ ^oC$
Al2024	0.4	2,600	900.0	121.0
Ti64	0.8	4,430	526.3	6.7
In718	0.8	8,190	435.0	11.4

The test-measured effective TQC tables of Al2024, Ti64, and In718 from the tensile tests were shown in Table 1. However, these values cannot be directly used as *MAT_224 input for two reasons. The first reason is that the data points in the measured effective TQC table obtained from tests are too sparse and deviated to define a smooth TQC vs. rate curve. The other, more fundamental reason is that because of no heat conduction, the temperature versus strain curve from low rate *MAT_224 simulations is increasing linearly, with increasing slope. However, in the actual low rate experiments, due to heat conduction, the temperature versus strain curve has a decreasing slope with increasing temperature. Therefore, the effective TQC values at low rates need to be calibrated for *MAT_224 input.

4 Methodology

The thermal softening of a material can be analyzed by a thermal-structural coupled simulation analysis method in which the structural solver calculates material deformation, and the thermal solver obtains temperature change by heat generation and conduction. Coupled thermal-structural analysis is known to have the capability to make accurate deformation and temperature predictions in metallic materials, achieving good agreement with material tests.

Structural-only analysis reduces simulation runtime significantly but does not include heat conduction. In a structural-only simulation, the *MAT_224 constitutive material model contains the feature to calculate temperature increases induced by plastic deformation, which allows the thermal softening analysis. However, because *MAT_224 does not have an independent heat conduction feature, the results between the thermal-structural coupled analysis and structural-only analysis are different at low and intermediate rates. So, the effective TQC values of *MAT_224 need to be calibrated to match structural-only analysis results with thermal-structural coupled analysis results.

In this study, a method to create the calibrated effective TQC table for *MAT_224 input was developed as a two-step approach. In the first step, the thermal-structural coupled solver is used to verify the physical TQC values of the materials by comparing numerical results with test results and create temperature curves at additional intermediate rates. In the second step, the structural-only solver is used to calibrate the effective TQC values at all rates and to validate the effective TQC table for input into *MAT_224.

4.1 Step 1: Thermal-structural coupled analysis

In the first step, the thermal-structural coupled solver is used in tensile test simulations to generate the temperature vs. strain curves at additional strain rates that were not covered by the physical tensile tests.

First, the material models of *MAT_224 that were developed using the structural-only solver need to be verified, confirming that they generate acceptable results in the thermal-structural coupled analysis. Especially, the referenced physical TQC values listed in Table 2 need to be verified to obtain accurate temperature results. It should be noted that in the LS-DYNA thermal-structural coupled solver, the physical TQC is defined by the FWORK parameter on the *CONTROL_THERMAL_SOLVER keyword input. The BETA parameter on the *MAT_224 keyword input is ignored when using the thermal-structural coupled solver.

All the physical tensile test series, at all the different rates, are simulated by the thermal-structural coupled solver. The outputs of simulations, such as force-displacement, temperature-strain, and rate-strain curves, are compared with test results to check the accuracy of simulations. Through iterative simulations, the physical TQC are adjusted to bring the simulation results closest to the test outputs.

Second, the additional simulations at extra rates are conducted with the adjusted physical TQC to obtain the additional temperature-strain curves, which provide additional points to the effective TQC table. The additional effective TQC values at extra rates make an effective TQC vs. strain rate curve smooth over the range of strain rates from isothermal to adiabatic.

4.2 Step 2: Structural-only analysis

In the second step, the structural-only solver is used to develop the effective TQC vs. strain rate table by calibrating the effective TQC values at each rate.

First, tensile test simulations at all rates were conducted by the structural-only solver to obtain their temperature-strain curves. In the structural-only analysis, the adjusted physical TQC in the first step was initially applied to the BETA parameter in *MAT_224. The adjusted physical TQC would work for the high-rate simulations but would not for lower rates due to the absence of heat conduction in the structural-only analysis. So, the BETA parameter needs to be calibrated to make temperature-strain curves obtained from the first and second steps comparable to each other.

Figure 4 shows the temperature-strain curves at the SR2 rate obtained from the first and second steps. The temperature-strain curve from the first step shows that the temperature increase slope is decreasing due to heat conduction, but the temperature-strain curves from the second step show nearly linear curves with different slopes depending on the BETA parameter values. These temperature-strain curves have a linear slope because of the absence of heat conduction in the structural-only analysis. So, it is difficult to compare the two curves directly because of the different trends. Instead, the areas under the curves up to a strain of 0.3 can be compared.

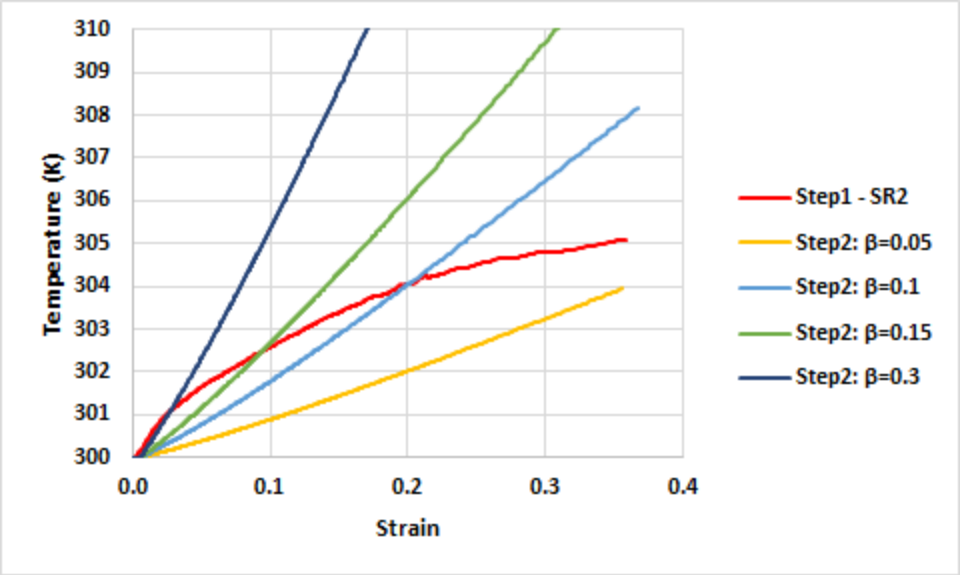

Figure 4. Temperature vs strain curves of Al2024 at SR2 obtained from the first and second steps

To calibrate the effective TQCs at each rate, the BETA parameter in *MAT_224 can be adjusted through iterative simulations to make two temperature-strain curves from the first and second steps comparable. Alternatively, an approximate method was developed to find the calibrated effective TQCs at each rate by utilizing the linearity of temperature-strain curves in the structural-only analysis. The areas under the temperature-strain curves with different BETA parameter values were also linearly proportional to the BETA parameter values, and so the slope of the area-BETA curve could be obtained. Because the goal was that the areas of the temperature-strain curves from the first and second steps should be the same, the calibrated effective TQC could be estimated by dividing the area of the temperature-strain curve from the first step by the slope of the area-BETA curve from the second step.

The calibrated effective TQC table was then developed by gathering the calibrated effective TQCs at all rates. The calibrated effective TQC table could then be validated by comparing its results with physical test results.

5 Finite element model and simulation

The Finite Element (FE) model of the tensile test coupon specimen was developed as shown in Figure 5. Its dimensions were summarized in Figure 1. The smallest solid element sizes are about 0.152 mm for Al2024, 0.145 mm for Ti64, and 0.137 mm for In718. The *MAT_224 material models of Al2024, Ti64, and In718 were used. Thermal material parameters for the *MAT_THERMAL_ISOTROPIC input in the thermal-structural coupled analysis were listed in Table 2. The initial temperature for all simulations was set to 300 degrees Kelvin because the physical tests were conducted at room temperature. In the tensile simulations, the strain was obtained by comparing displacements from two nodes, matching the test Digital Image Correlation (DIC) virtual extensometer length shown in Figure 5. The temperature was measured at the center of the specimen where the material failure was initiated. The strain rate curves were obtained by differentiating the strain curves and taking their moving averages to remove noise.

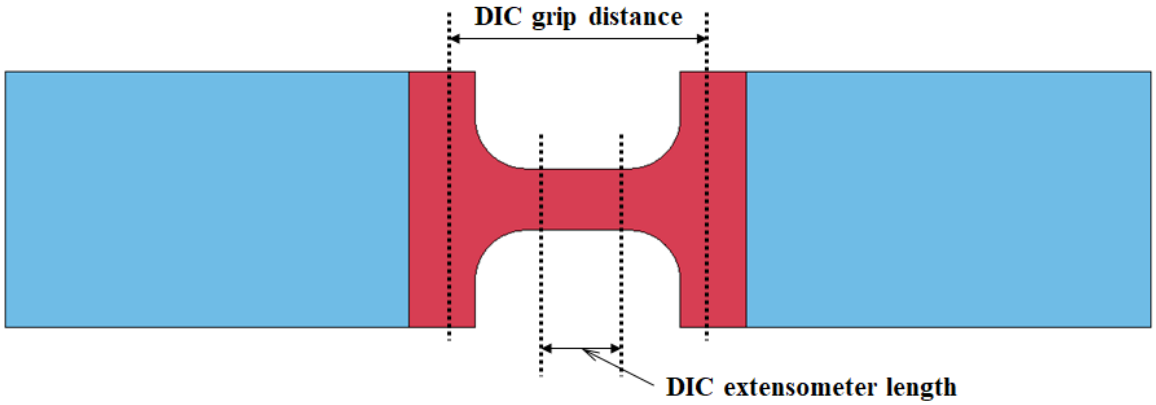

Figure 5. FE model of the tensile test specimen

The physical tensile tests were conducted at six different strain rates, ranging from quasi-static to high rates, as shown in Table 1. To simulate them efficiently, the LS-DYNA implicit structural solver was used for quasi-static to low rates, and the LS-DYNA explicit structural solver was used for mid to high rates. In the implicit analysis, a convergence study was conducted to check simulation accuracy.

In the physical mid to high-rate tensile tests, grip slippage often occurs, and displacements measured away from the specimen are then inaccurate. The uncertain condition in these specimens makes developing accurate material models problematic. In the tests, the DIC camera frame was set up to capture the displacements of both grip locations. Then, the grip displacement history was measured from the DIC image and applied in the simulations as a loading condition, directly at the grip locations, as shown in Figure 5.

Two FE models of the test specimen were developed. One is a short FE model which only modeled the red area in Figure 5. To reduce runtime, the long grip area of a tensile specimen, where no deformation occurs, is typically not modeled. However, at low rates, in the thermal-structural coupled analysis the grip area plays an important role in heat conduction. So, the long FE model which includes the blue grip area in Figure 5 is used, allowing thermal energy to conduct into the grip sections. In addition, heat convection plays a role in the thermal-structural coupled analysis at quasi-static rates. Thus, a heat convection boundary condition was applied with the convection heat transfer coefficient of 5 W/m^2-K (free convection in the air). Figure 6 shows how the temperature of an Al2024 specimen changes in the thermal-structural coupled analysis at the SR1 rate, adding grip modeling for heat conduction and a heat convection boundary condition.

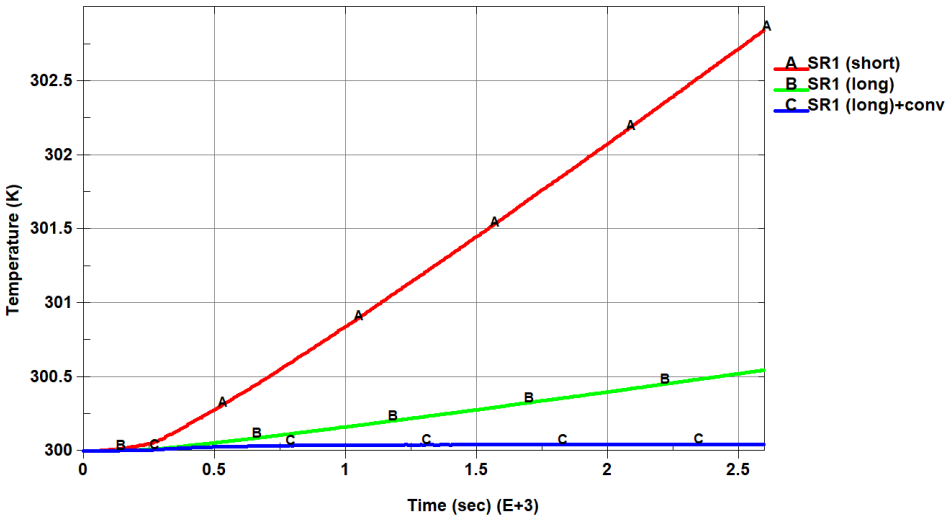

Figure 6. Temperature curves of a Al2024 specimen in the thermal-structural coupled analysis at SR1

6 Effective TQC table creation

The effective TQC tables for *MAT_224 material models of Al2024, Ti64, and In718 were created and validated using the method described above. Simulation results using these tables are summarized in this section. It should be noted that those previously existing metallic material models of *MAT_224 were developed when less test data was available, including no thermal data, and so the referenced physical TQC values were not verified at that time. Therefore, it was not expected that all simulation outputs would agree well with the physical test data.

6.1 Al2024

The repeated thermal-structural coupled analyses in Step 1 determined that the adjusted physical TQC value of Al2024 is 0.5, which is higher than the 0.4 of the referenced physical TQC value shown in Table 2. The results of Al2024 tensile simulations at six test rates by the thermal-structural coupled analysis, using a physical TQC value of 0.5, are shown in Appendix A. Comparisons with the physical test results include force-displacement curves, temperature-strain curves, and rate-strain curves. Overall, the thermal-structural coupled analysis results in Step 1 are comparable to the test results, except that the simulated temperature rises at 0.3 strain in the SR2 and SR3 rates are 2 to 5 degrees Kelvin lower than in tests.

The additional rates, which were not covered by the physical tests and were added, are listed in Table 3. The thermal-structural coupled analyses at those rates generated the additional temperature-strain curves as shown in Figure 7. The selections of the analysis method and FE model at each rate are described in Table 3. The approximation method described in section 4.2 estimated the calibrated effective TQC values at every rate as summarized in Table 3. Figure 8 shows the calibrated effective TQC values vs. rate curve, which is the Al2024 calibrated effective TQC table for *MAT_224.

The comparison of the temperature-strain curves between the thermal-structural coupled analysis and the structural-only analysis with the calibrated effective TQC table is shown in Figure 9. The shapes of temperature curves between two analyses are different, but the area under the curves at strains less than 0.3 are comparable. The strain value of 0.3 is the approximate erosion strain under tension of the Al2024 *MAT_224 model.

Table 3. Summary of Al2024 simulations

Name		Actual rate (1/sec)	Calibrated effective TQC (β)	Analysis method	FE model
R.0001	SR1	1.00E-04	0.00	Implicit	long & convection
R.001		1.00E-03	0.01	Implicit	long & convection
R.01		1.00E-02	0.02	Implicit	long & convection
R.1	SR2	1.00E-01	0.08	Implicit	long
R.25		2.50E-01	0.15	Implicit	long
R.5		5.00E-01	0.21	Implicit	long
R1	SR3	1.00E+00	0.28	Implicit	short
R2.5		2.50E+00	0.37	Implicit	short
R5		5.00E+00	0.41	Implicit	short
R10		1.00E+01	0.44	Explicit	short
R100		1.00E+02	0.47	Explicit	short
R500	SR4	5.00E+02	0.48	Explicit	short
R2000	SR5	2.00E+03	0.49	Explicit	short
R6000	SR6	6.00E+03	0.50	Explicit	short

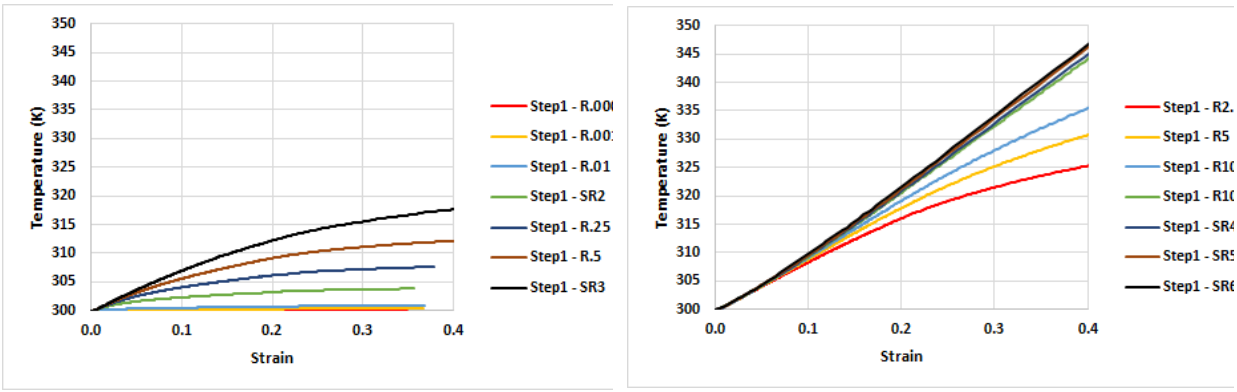

(a) lower strain rates (b) higher strain rates

Figure 7. Additional temperature vs. strain curves of Al2024

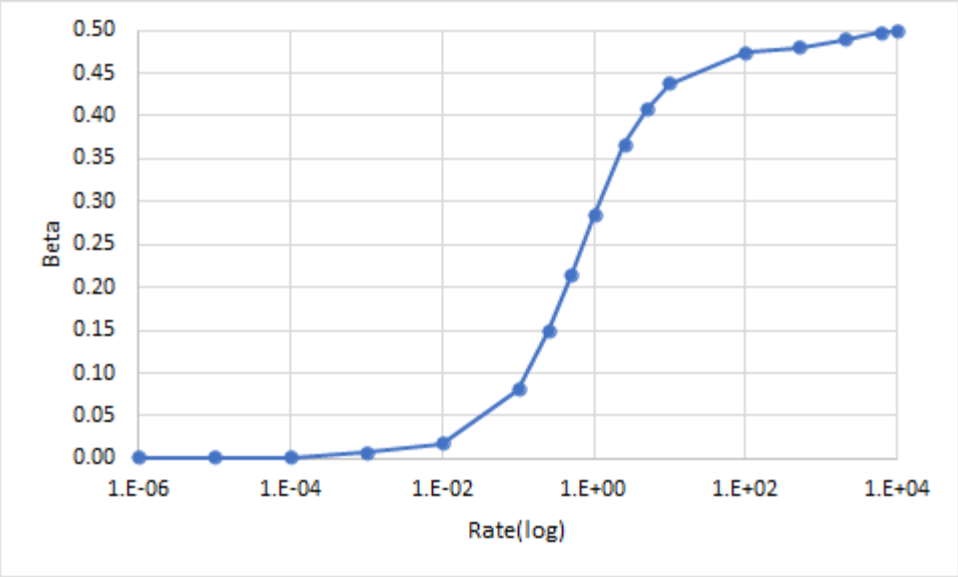

Figure 8. Calibrated effective TQC table of Al2024

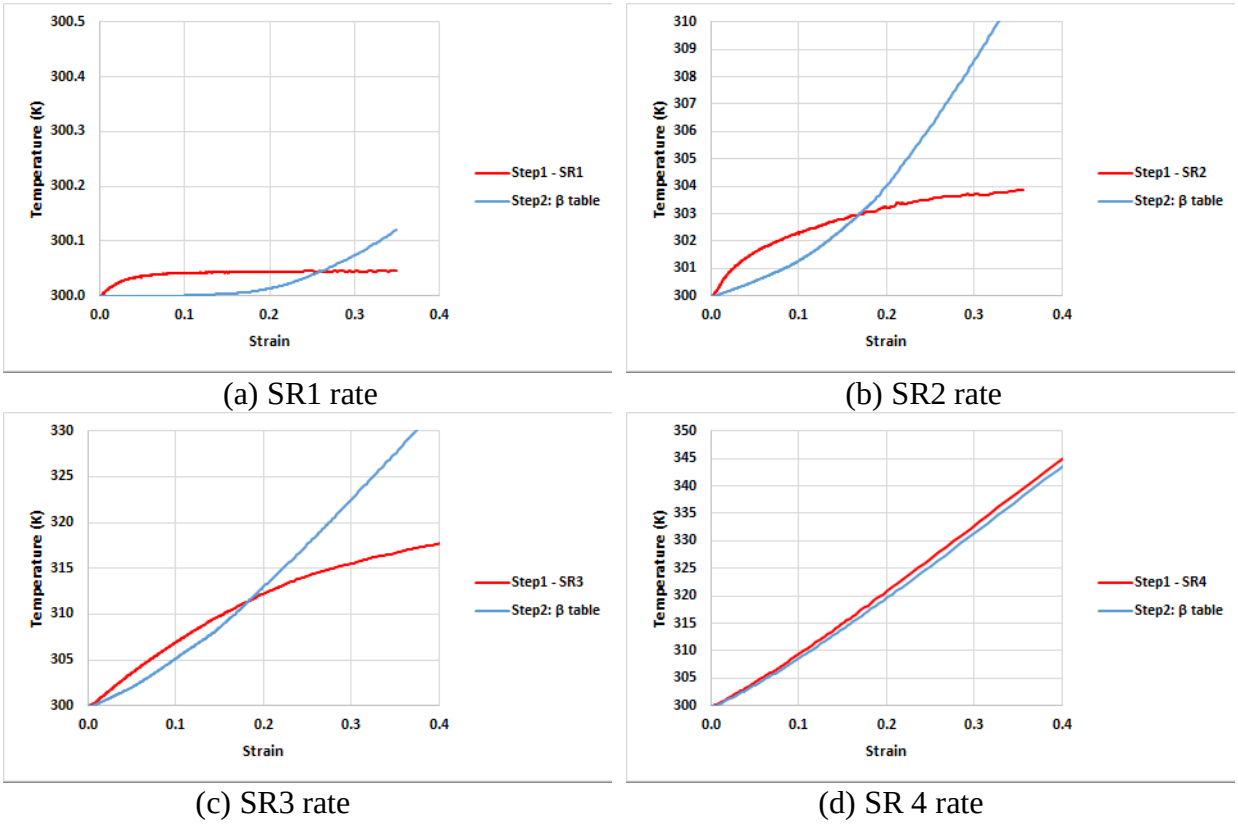

(a) SR1 rate

(b) SR2 rate

(c) SR3 rate

(d) SR 4 rate

Figure 9. Comparison of temperature vs. strain curves between thermal-structural coupled analysis (step 1) and structural-only analysis (step 2) on Al2024

6.2 Ti64

The repeated thermal-structural coupled analyses in Step 1 determined that the adjusted physical TQC value of Ti64 is 0.8, which is the same as the referenced physical TQC value shown in Thermal properties of Al2024, Ti64, and In718. The results of Ti64 tensile simulations at five test rates by the thermal-structural coupled analysis, using a physical TQC value of 0.8, are shown in Appendix B. Comparisons with the physical test results include force-displacement curves, temperature-strain curves, and rate-strain curves. In the force-displacement curves, the peak forces are similar between tests and simulations, but the forces are decreasing much slower in simulations as the displacements are increasing. So, the overall strains in simulations are much smaller, and the strain rates are also smaller in the rate-strain curves. This discrepancy between tests and simulations was likely caused by the relatively limited test data available when the *MAT_224-Ti64 dataset was developed. In the temperature-strain curves, however, the temperature increases between tests and simulations are close at all five rates.

The additional rates which were not covered by the physical tests and were added, are as listed in Table 4. The thermal-structural coupled analyses at those rates generated the additional temperature-strain curves as shown in Figure 10. The selections of the analysis method and FE model at each rate are described in Table 4. The approximation method estimated the calibrated effective TQC values at every rate as summarized in Table 4. Figure 11 shows the calibrated effective TQC values vs. rate curve, which is the Ti64 calibrated effective TQC table for *MAT_224. The comparison of the temperature-strain curves between the thermal-structural coupled analysis and the structural-only analysis with the calibrated effective TQC table is shown in Figure 12.

Table 4. Summary of Ti64 simulations

Name		Actual rate (1/sec)	Calibrated effective TQC (β)	Analysis method	FE model
R.0001	SR1	1.00E-04	0.00	Implicit	long & convection
R.001		1.00E-03	0.02	Implicit	long & convection
R.01		1.00E-02	0.14	Implicit	long & convection
R.1	SR2	1.00E-01	0.43	Implicit	short
R.25		2.50E-01	0.56	Implicit	short
R.5		5.00E-01	0.64	Implicit	short
R1	SR3	1.00E+00	0.67	Implicit	short
R2.5		2.50E+00	0.67	Implicit	short
R5		5.00E+00	0.67	Implicit	short
R10		1.00E+01	0.70	Explicit	short
R100		1.00E+02	0.73	Explicit	short
R500	SR4	7.00E+02	0.76	Explicit	short
R2000	SR5	2.20E+03	0.80	Explicit	short

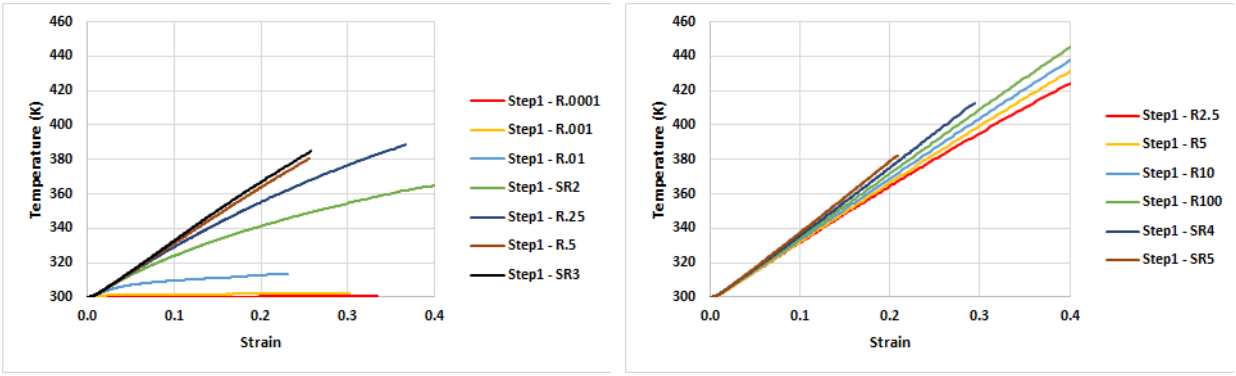

(a) lower rates (b) higher rates

Figure 10. Additional temperature vs. strain curves of Ti64

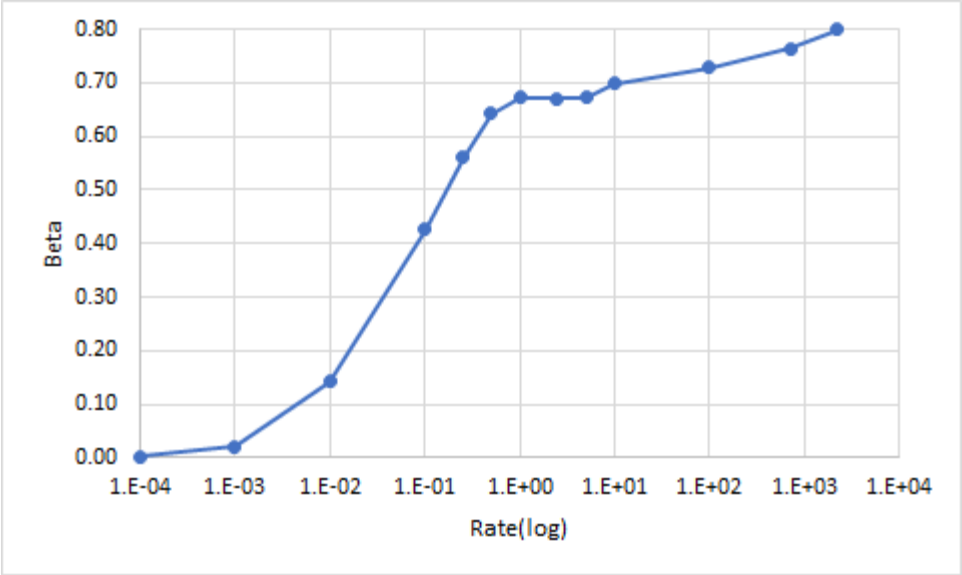

Figure 11. Calibrated effective TQC table of Ti64

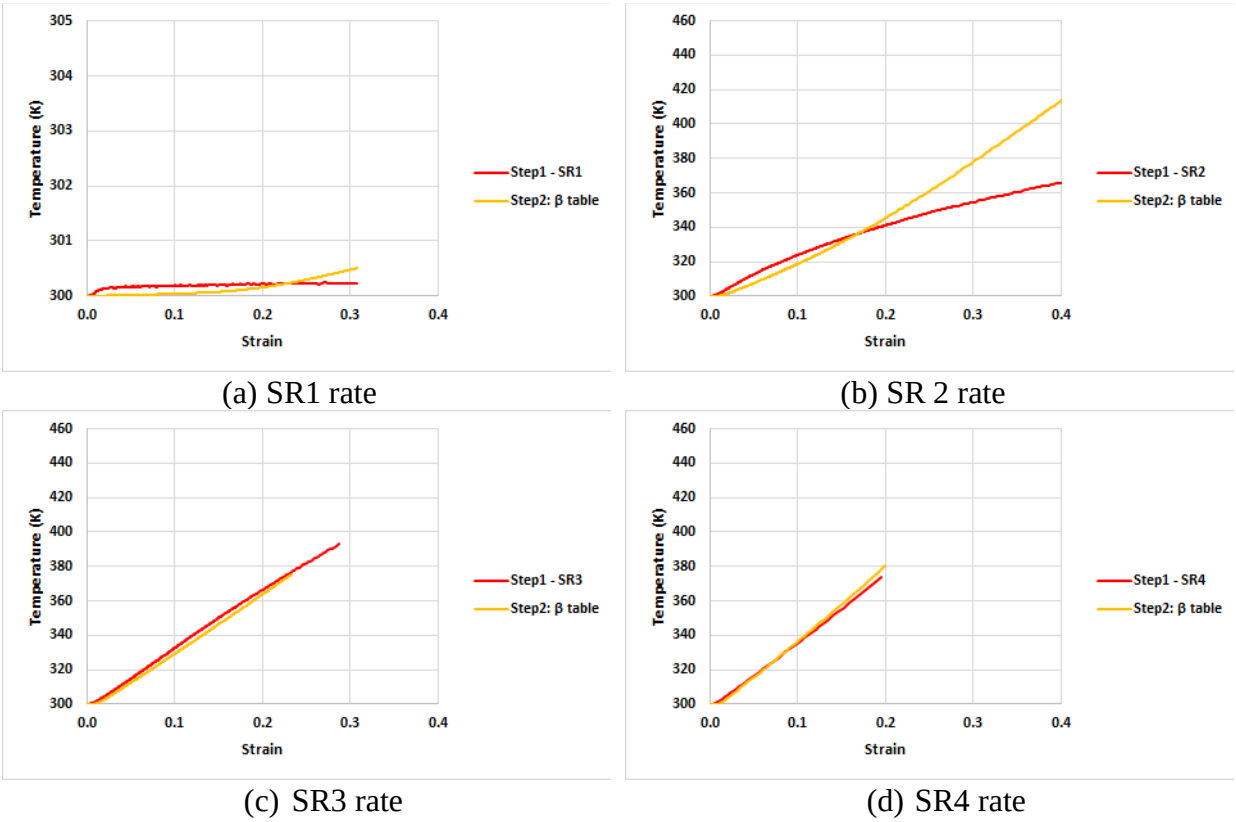

(a) SR1 rate (b) SR 2 rate

(c) SR3 rate (d) SR4 rate

Figure 12. Comparison of temperature vs. strain curves between thermal-structural coupled analysis (step 1) and structural-only analysis (step 2) for Ti64

6.3 In718

The repeated thermal-structural coupled analyses in Step 1 determined that the adjusted physical TQC value of In718 is 0.7, which is lower than the 0.8 of the referenced physical TQC value shown in Table 2. The results of In718 tensile simulations at five test rates by the thermal-structural coupled analysis, using a physical TQC value of 0.7, are shown in Appendix C. Comparisons with the physical test results include force-displacement curves, temperature-strain curves, and rate-strain curves. Overall, the thermal-structural coupled analysis results in Step 1 are comparable to the test results at all five rates.

The additional rates, which were not covered by the physical tests and were added, are listed in Table 5. The thermal-structural coupled analyses at those rates generated the additional temperature-strain curves as shown in Figure 13. The selections of the analysis method and FE model at each rate are described in Table 5. The approximation method estimated the calibrated effective TQC values at every rate as summarized in Table 5. Figure 14 shows the calibrated effective TQC values vs. rate curve, which is the In718 calibrated effective TQC table, for *MAT_224. The comparison of the temperature-strain curves between the thermal-structural coupled analysis and the structural-only analysis with the calibrated effective TQC table is shown in Figure 15.

Table 5. Summary of In718 simulations

Name		Actual rate (1/sec)	Calibrated effective TQC (β)	Analysis method	FE model
R.0001	SR1	1.00E-04	0.00	Implicit	long & convection
R.001		1.00E-03	0.02	Implicit	long & convection
R.01		1.00E-02	0.12	Implicit	long & convection
R.1	SR2	1.00E-01	0.45	Implicit	short
R.25		2.50E-01	0.55	Implicit	short
R.5		5.00E-01	0.60	Implicit	short
R1	SR3	1.00E+00	0.63	Implicit	short
R2.5		2.50E+00	0.64	Implicit	short
R5		5.00E+00	0.65	Implicit	short
R10		1.00E+01	0.66	Explicit	short
R100		1.00E+02	0.67	Explicit	short
R500	SR4	5.60E+02	0.68	Explicit	short
R2000	SR5	2.20E+03	0.70	Explicit	short

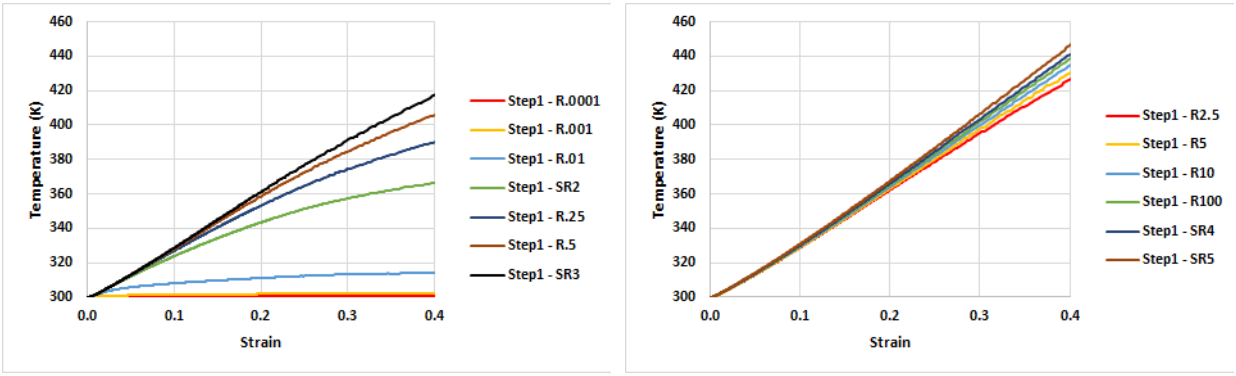

(a) lower rates (b) higher rates

Figure 13. Additional temperature vs. strain curves of In718

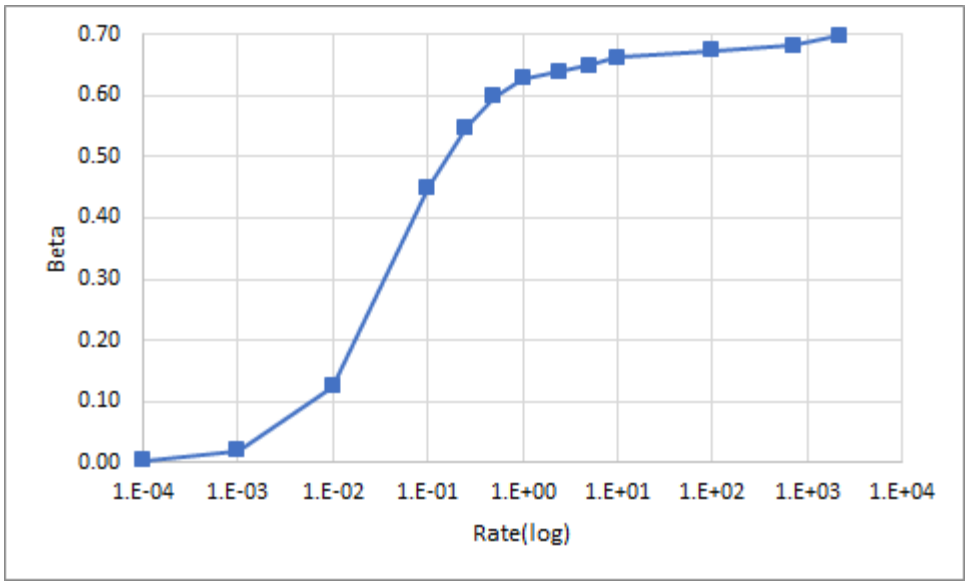

Figure 14. Calibrated effective TQC table of In718

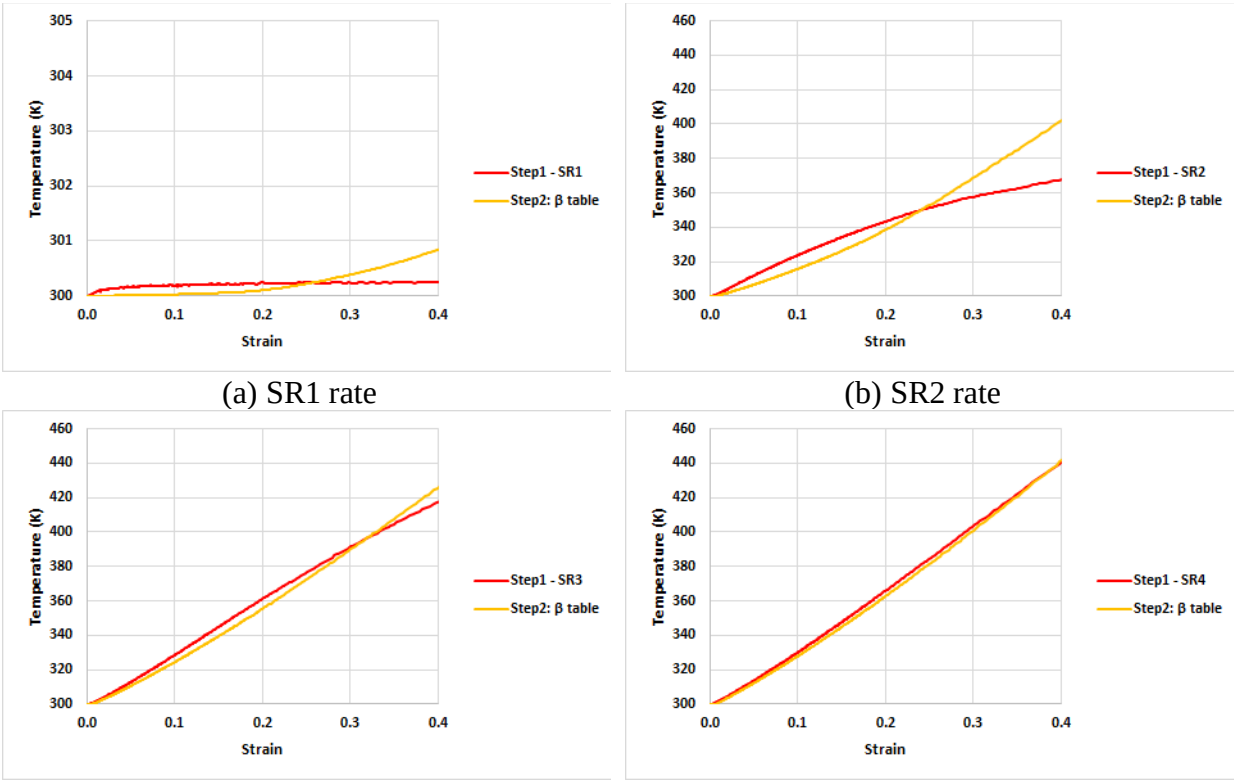

(a) SR1 rate (b) SR2 rate

(c) SR3 rate (d) SR4 rate

Figure 15. Comparison of temperature vs. strain curves between thermal-structural coupled analysis (step 1) and structural-only analysis (step 2) on In718

6.4 Summary

Figure 16 summarizes all the different TQCs for all three metallic materials. First, the green curves in Figure 16 show the referenced constant, physical TQC of the current three metallic *MAT_224 material models. The measured, effective TQC values, at different rates obtained from the physical tensile tests, are the red dots in Figure 16. The TQC table, the blue curves in Figure 16, is the calibrated, effective TQC curves obtained from simulations. It is observed that the measured TQC red dots correlate with the TQC table curves, with some deviation. The trends show that the TQC table curve could be fitted with a logistic function. The typical logistic function $f(x)$ is expressed as Equation 4, where L is the maximum value, k is the growth rate, and x_0 is the midpoint.

$$f(x) = \frac{L}{1+e^{-k(x-x_0)}} \quad (4)$$

The logistic function curves, the yellow curves in Figure 16, are obtained with the fitting parameters shown in Table 6. The logistic function curves are very close to the TQC table curves in the low to mid-rate ranges, but they show some difference in the mid to high-rate ranges.

Table 6. Summary of logistic function parameters

	Al2024	**Ti64**	**In718**
L	0.5	0.8	0.7
k	1.8	1.7	2.1
x_0	-0.1	-1.1	-1.3

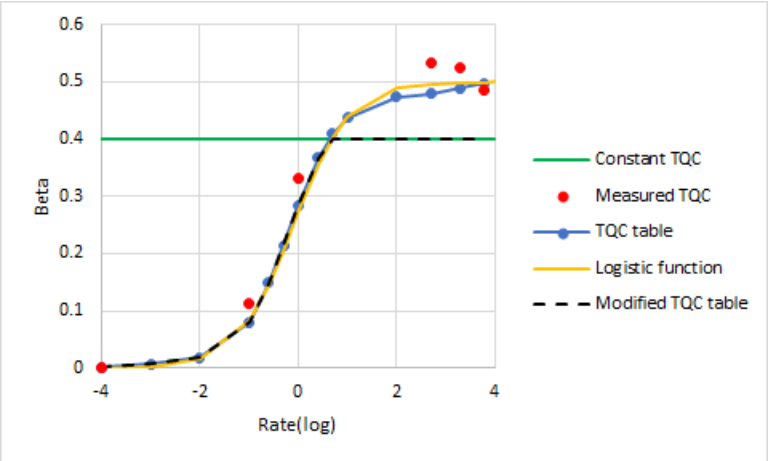

(a) Al2024

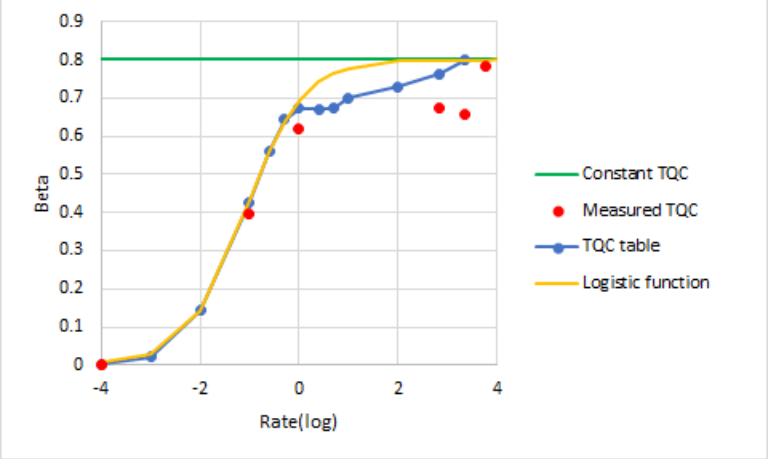

(b) Ti64

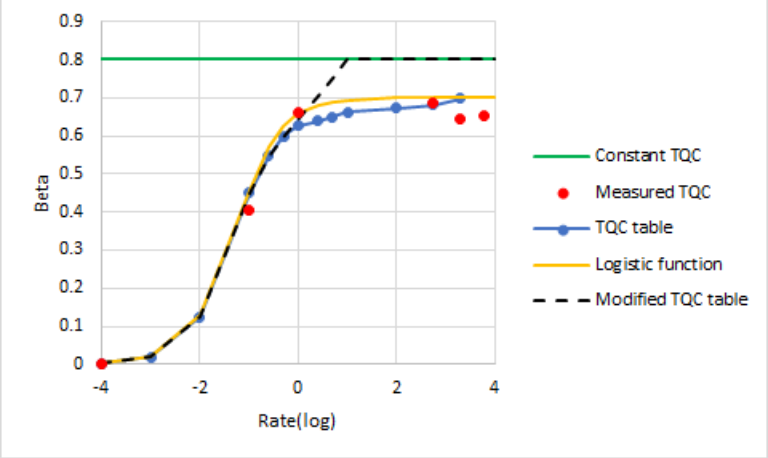

(c) In718

Figure 16. Summary of TQCs for Al2024, Ti64, and In718

The original intention was to replace the constant TQC with the developed TQC tables. However, the adjusted physical TQC values of Al2024 and In718, which are the highest values in the TQC tables, are different from the referenced constant, physical TQC values. So, if the constant TQCs are replaced with the TQC tables directly, this change could be problematic for backward compatibility. Because the material datasets were developed based on the referenced physical TQC values, using the TQC table directly might cause simulation mismatches with ballistic test data. Therefore, at the highest strain rates in the Al2024 and In718 TQC tables, the verified physical TQC values were modified to match the referenced physical TQC values. This final revision produces the modified effective TQC tables, the black dotted curves in Figure 16(a) and Figure 16(c). The TQC table of Ti64 does not need to be modified because the constant TQC and the verified physical TQC value are the same at the highest strain rates.

7 Conclusions

In this research work, the effective TQC tables of *MAT_224 for Al2024, Ti64, and In718 were developed to replace the current constant TQCs. The current constant TQCs can be problematic for both ballistic impact simulations in regions away from the impact, and for simulating longer duration events such as engine rundown and windmilling, where there are low and intermediate strain rates present. When and where strain rates are low and intermediate, heat conduction lessens temperature rise and thermal softening. The effective TQC tables presented here compensate for heat conduction by lowering the amount of heat initially generated.

The methodology to create the effective TQC table was developed by using a two-step approach. In Step 1, the thermal-structural analyses of tensile tests were conducted to verify the referenced TQC values and generate additional temperature-strain curves at additional rates that were not covered by the physical tensile tests. In Step 2, the structural-only analyses of tensile tests were conducted to calibrate the effective TQC values at all the rates for the effective TQC table, and to validate the calibrated effective TQC table.

The thermal-structural coupled analyses demonstrated that the verified physical TQC values were higher than the referenced physical TQC values of Al2024 and lower than those of In718. Also, they showed that some differences between the results of the physical tests and the simulations were apparent. These discrepancies could be due to the relatively limited test data available when those material models were developed, such as no thermal test data. So, to improve the accuracy of *MAT_224 material models, it is suggested that in the future effective TQC table creation should be integrated in the development process of any new *MAT_224 material dataset.

The use of an effective TQC table provides a way to overcome the absence of heat conduction in structural-only analysis using *MAT_224, so that *MAT_224 can be used for applications at low rates, as well as high rates. However, the inherent limitations of *MAT_224 still remain. For instance, heat dissipation is dependent on material geometry and surrounding initial and boundary conditions, which means that effective TQC tables would theoretically need to be changed with different surrounding environments. One possible resolution, avoiding a computationally costly coupled thermal-structural analysis, would be to implement heat conductivity into the *MAT_224 constitutive model. This resolution could follow the proposed numerical approach to describe heat conduction terms in Equation 1, with the help of a finite difference quotient (BehrensB.-A., ChugreevA., BohneF., LorenzR., 2019).

8 References

Behrens, B.-A., Chugreev, A., Bohne, F., & Lorenz, R. (2019). Approach for modelling the Taylor-Quinney coefficient of high strength steels. *Procedia Manufacturing, 29*, 464-471.

Buyuk, M. (2014). *Development of a New Metal Material Model in LS-DYNA, Part 2: Development of a Tabulated Thermo-Viscoplastic Material Model with Regularized Failure for Dynamic Ductile Failure Prediction of Structures under Impact Loading.* Final Report, Federal Aviation Administration, U.S. Department of Transportation. Retrieved from https://www.tc.faa.gov/its/worldpac/techrpt/tc13-25p2.pdf

Dolci, S. (2022). *The Influence of Strain Rate, Temperature Effects, and Instabilities in Failure Modeling for Metal Alloys.* Technical Thesis, Federal Aviation Administration, U.S. Department of Transportation. Retrieved from https://www.tc.faa.gov/its/worldpac/techrpt/tctt22-21.pdf

Dolci, S., Carney, K., Wang, L., Du Bois, P., & Kan, C. (2023 expected). *Development of a Inconel Alloy Inco-718 Material Model Used in LS-DYNA.* Final Report, Federal Aviation Administration, U.S. Department of Transportation.

Emmerling, W., Altobelli, D., Carney, K., & Pereira, M. (2014). *Development of a New Metal Material Model in LS-DYNA, Part 1: FAA, NASA, and Industry Collaboration Background.* Technical Report, Federal Aviation Administration, U.S. Department of Transportation. Retrieved from https://www.tc.faa.gov/its/worldpac/techrpt/tc13-25-p1.pdf

Haight, S., Wang, L., Du Bois, P., Carney, K., & Kan, C. D. (2016). *Development of a Titanium Alloy Ti-6Al-4V Material Model Used in LS-DYNA.* Final Report, Federal Aviation Administration, U.S. Department of Transportation. Retrieved from https://www.tc.faa.gov/its/worldpac/techrpt/tc15-23.pdf

Hammer, J. T. (2014). *Plastic Deformation and Ductile Fracture of Ti-6Al-4V under Various Loading Conditions.* Technical Thesis, Federal Aviation Administration, U.S. Department of Transportation. Retrieved from https://www.tc.faa.gov/its/worldpac/techrpt/tctt14-2.pdf

Kelley, S., & Johnson, G. (2006). *Statistical Testing of Aircraft Materials for Transport Airplane Rotor Burst Fragment Shielding.* Final Report, Federal Aviation Administration, U.S.

Department of Transportation. Retrieved from https://www.tc.faa.gov/its/worldpac/techrpt/AR06-9.pdf

LS-DYNA Aerospace Working Group. (2023). Retrieved from https://awg.ansys.com/Material+Parameter+Sets

LSTC. (2017). *LS-DYNA Keyword User's Manual, Volume I and II, Version R10.0.* Livermore, California: Livermore Software Technology Corporation.

Park, C. K., Carney, K., Du Bois, P., Cordasco, D., & Kan, C. D. (2020). *Aluminum 2024-T351 Input Parameters for *MAT_224 in LS-DYNA.* Final Report, Federal Aviation Adminstration, U.S. Department of Transportation. Retrieved from https://www.tc.faa.gov/its/worldpac/techrpt/tc19-41-p1.pdf

Park, C. K., Queitzsch, G., Carney, K., Du Bois, P., Kan, C. D., Cordasco, D., & Emmerling, W. (2020). *Aluminum 2024-T351 Input Parameters for *MAT_224 in LS-DYNA, Part 3: Ballistic Impact Simulations of an Aluminum 2024 Panel Using *MAT_224 in LS-DYNA Considering Oblique Incidence and Attitude Angles of a Rectangular Projectile.* Final Report, Federal Aviation Administration, U.S. Department of Transportation. Retrieved from https://www.tc.faa.gov/its/worldpac/techrpt/tc19-41-p3.pdf

Park, C., Carney, K., Du Bois, P., Kan, C., & Cordasco, D. (2021). *Aluminum 2024-T351 Input Parameters for *MAT_224 in LS-DYNA, Part 4: Ballistic Impact Simulations of a Titanium 6Al-4V Generic Fan Blade Fragment on an Aluminum 2024 Panel Using *MAT_224 in LS-DYNA.* Final Report, Federal Aviation Administration, U.S. Department of Transportation. Retrieved from https://www.tc.faa.gov/its/worldpac/techrpt/tc19-41-p4.pdf

Pereira, M., Revilock, D., Lerch, B., & Ruggeri, C. (2013). *Impact Testing of Aluminum 2024 and Titanium 6Al-4V for Material Model Development.* Technical Memorandum, National Aeronautics and Space Administration. Retrieved from https://ntrs.nasa.gov/citations/20130013684

Ravichandran, G., Rosakis, A. J., Hodowany, J., & Rosakis, P. (2002). On the conversion of plastic work into heat during high-strain-rate deformation. *AIP Conference Proceedings, 620*, pp. 557-562.

Seidt, J. D. (2014). *Development of a New Metal Material Model in LS-DYNA, Part 3: Plastic Deformation and Ductile Fracture of 2024 Aluminum under Various Loading Conditions.*

Final Report, Federal Aviation Administration, U.S. Department of Transportation. Retrieved from https://www.tc.faa.gov/its/worldpac/techrpt/tc13-25-p3.pdf

Seidt, J. D., Park, C., Buyuk, M., Lowe, R. L., Wang, L., Carney, K. S., . . . Kan, C. (2022). An Experimental Investigation of the Influence of the State of Stress on the Ductile Fracture of 2024-T351 Aluminum. *ASME Journal of Engineering Materials and Technology, 144*, 041006-1.

Seidt, J. D., Smith, J. L., Spulak, N., Lowe, R. L., & Gilat, A. (2022). *Aluminum 2024-T351 Input Parameters for *MAT_224 in LS-DYNA, Part 2: Additional tests to determine plastic heating and ductile fracture behavior under combined loading.* Federal Aviation Administration, U.S. Department of Transportation. Retrieved from https://www.tc.faa.gov/its/worldpac/techrpt/tc19-41-p2.pdf

Smith, J. L. (2019). *Full-Field Measurement of the Taylor-Quinney Coefficient in Tension Tests of Ti-6Al-4V, Aluminum 2024-T351, and Inconel 718 at Various Strain Rates.* Technical Thesis, Federal Aviation Administration, U.S. Department of Transportation. Retrieved from https://www.tc.faa.gov/its/worldpac/techrpt/tctt20-40.pdf

A Al2024 tensile test simulation results in Step 1

Figure A-1. Comparison between tests and thermal-structural coupled simulations for Al2024 at the SR1 rate A-2
Figure A-2. Comparison between tests and thermal-structural coupled simulations for Al2024 at the SR2 rate A-3
Figure A-3. Comparison between tests and thermal-structural coupled simulations for Al2024 at the SR3 rate A-4
Figure A-4. Comparison between tests and thermal-structural coupled simulations for Al2024 at the SR4 rate A-5
Figure A-5. Comparison between tests and thermal-structural coupled simulations for Al2024 at the SR5 rate A-6
Figure A-6. Comparison between tests and thermal-structural coupled simulations for Al2024 at the SR6 rate A-7

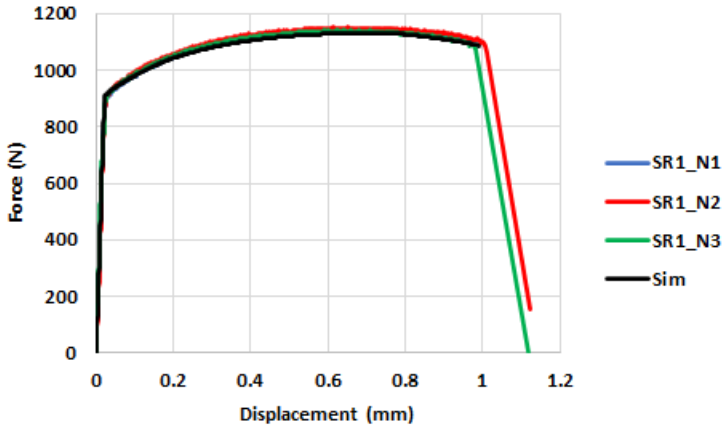

(a) force vs. displacement

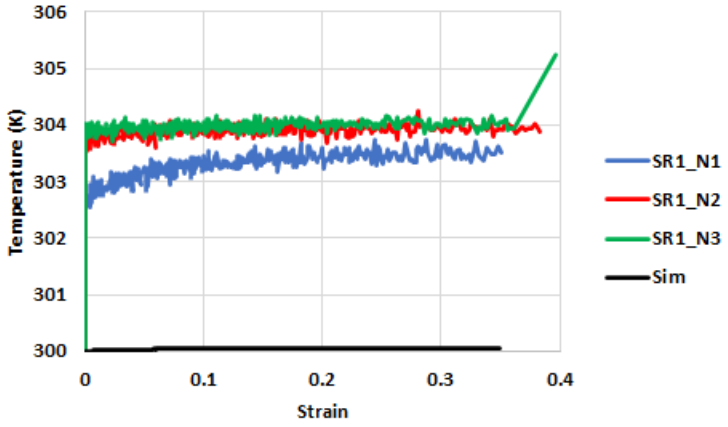

(b) temperature vs. strain

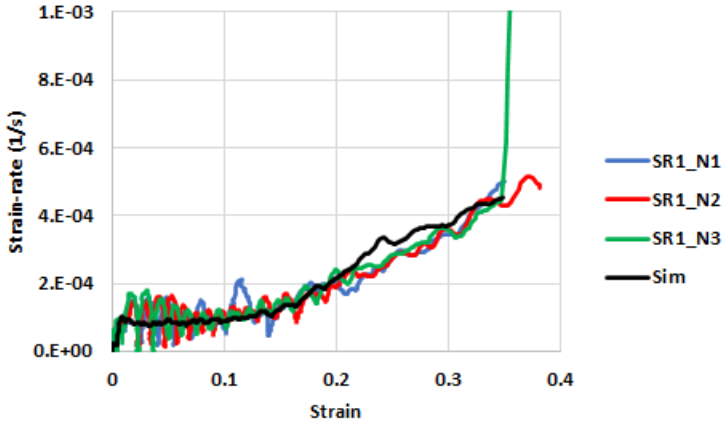

(c) strain rate vs. strain

Figure A-1. Comparison between tests and thermal-structural coupled simulations for Al2024 at the SR1 rate

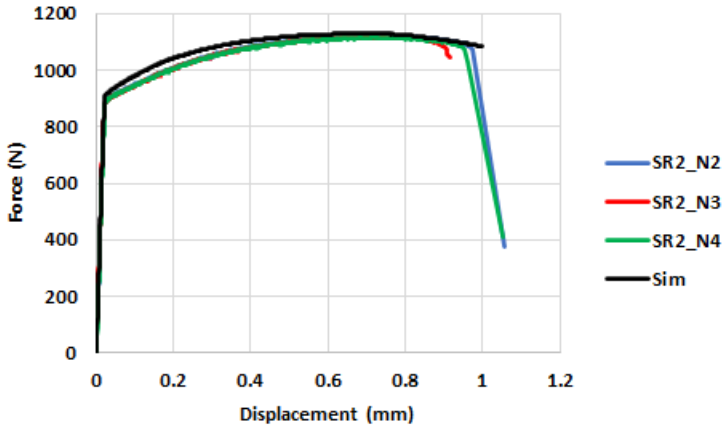

(a) force vs. displacement

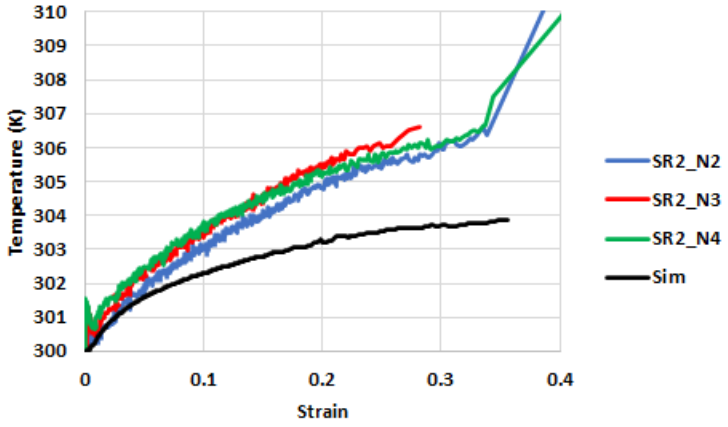

(b) temperature vs. strain

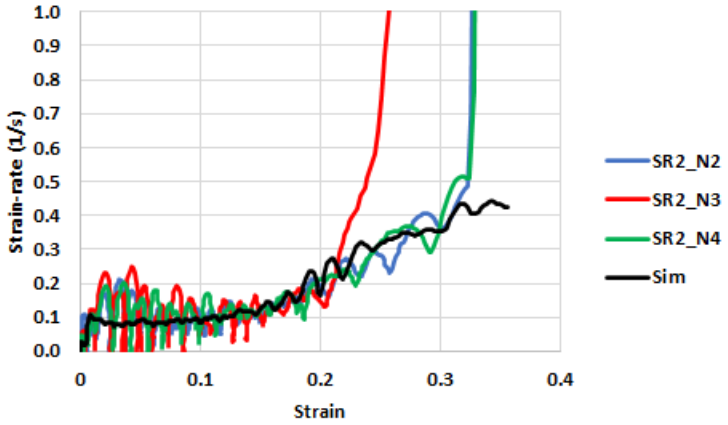

(c) strain rate vs. strain

Figure A-2. Comparison between tests and thermal-structural coupled simulations for Al2024 at the SR2 rate

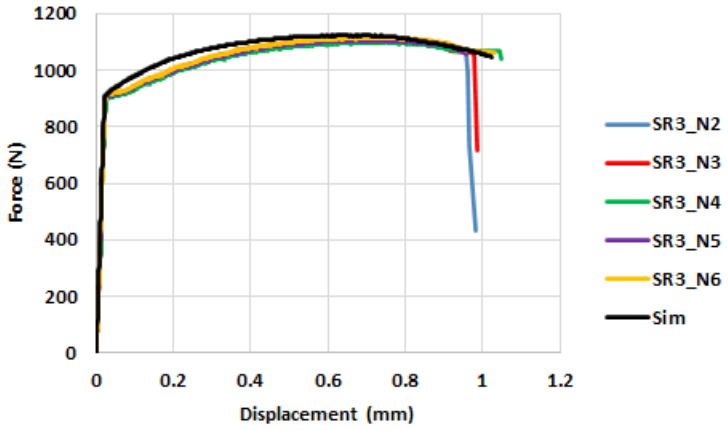

(a) force vs. displacement

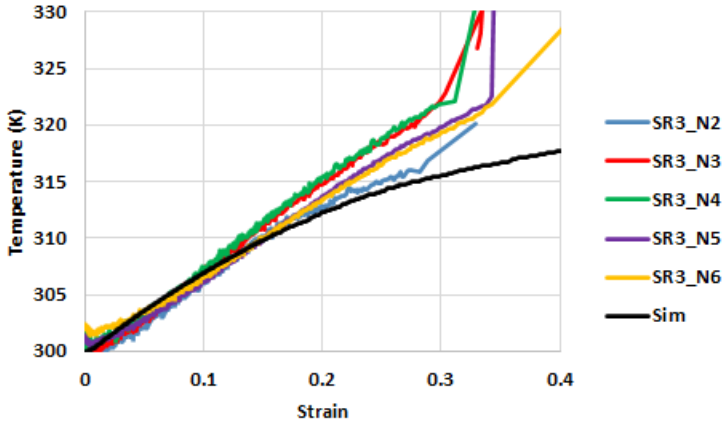

(b) temperature vs. strain

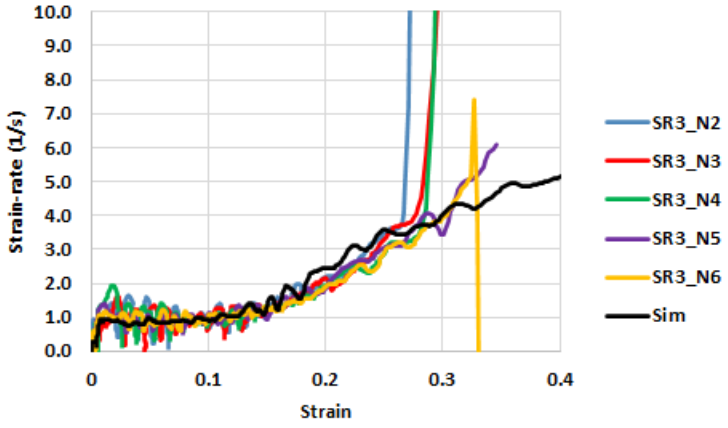

(c) strain rate vs. strain

Figure A-3. Comparison between tests and thermal-structural coupled simulations for Al2024 at the SR3 rate

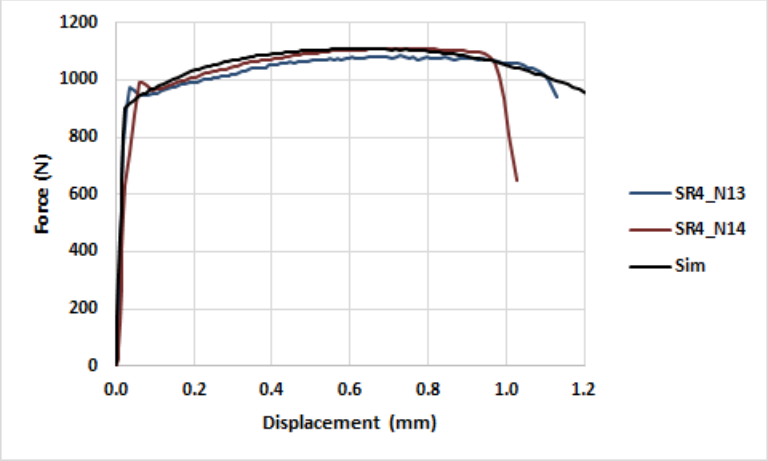

(a) force vs. displacement

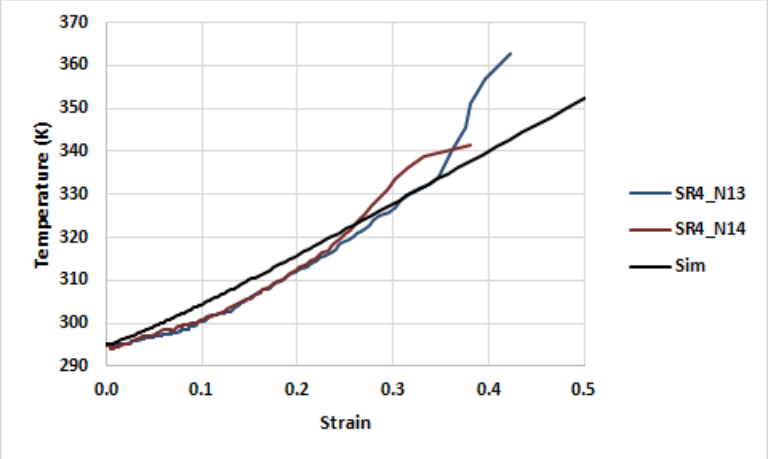

(b) temperature vs. strain

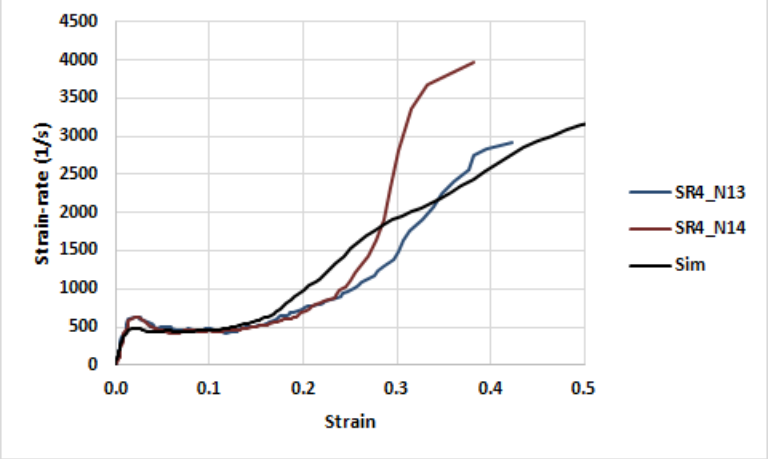

(c) strain rate vs. strain

Figure A-4. Comparison between tests and thermal-structural coupled simulations for Al2024 at the SR4 rate

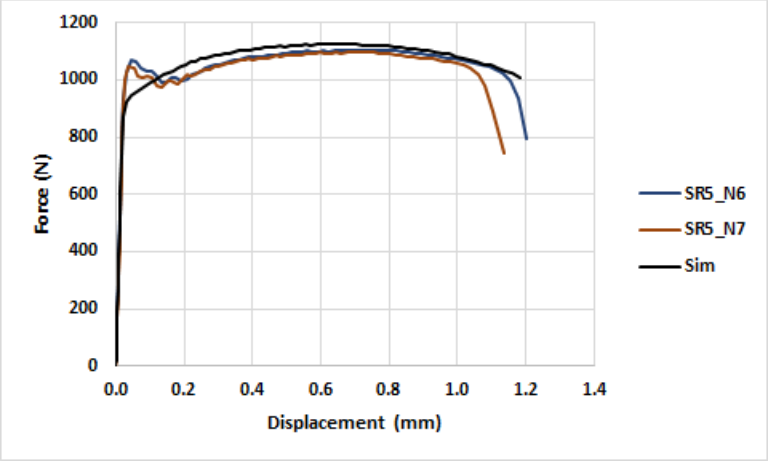

(a) force vs. displacement

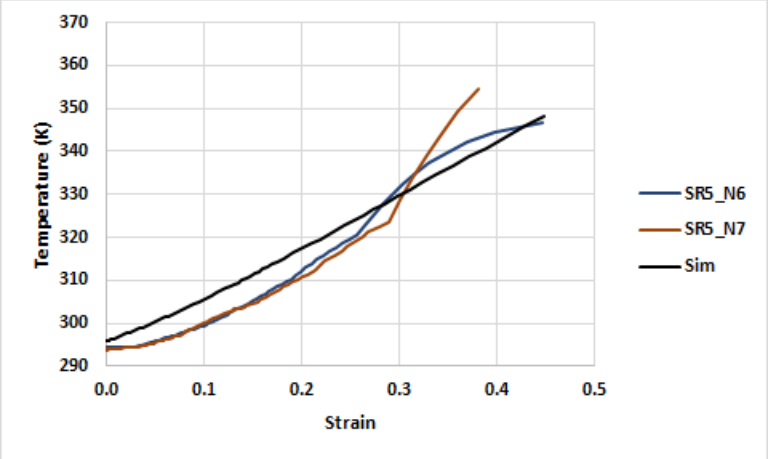

(b) temperature vs. strain

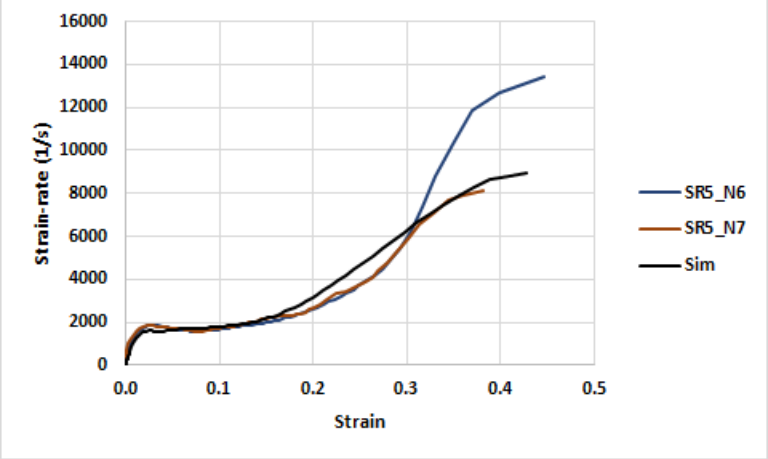

(c) strain rate vs. strain

Figure A-5. Comparison between tests and thermal-structural coupled simulations for Al2024 at the SR5 rate

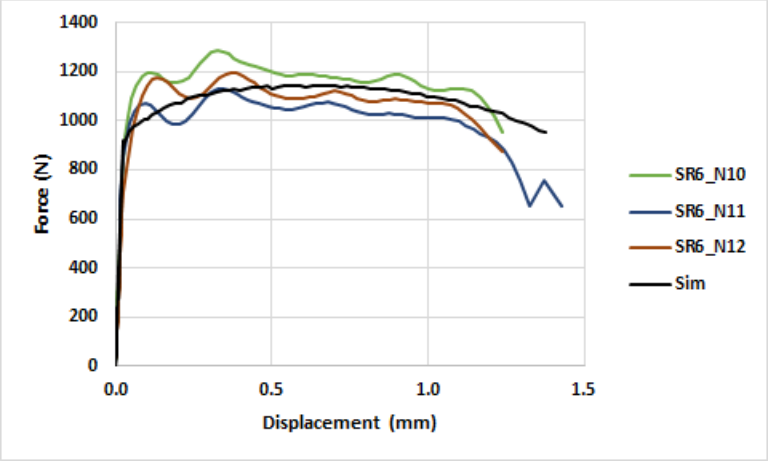

(a) force vs. displacement

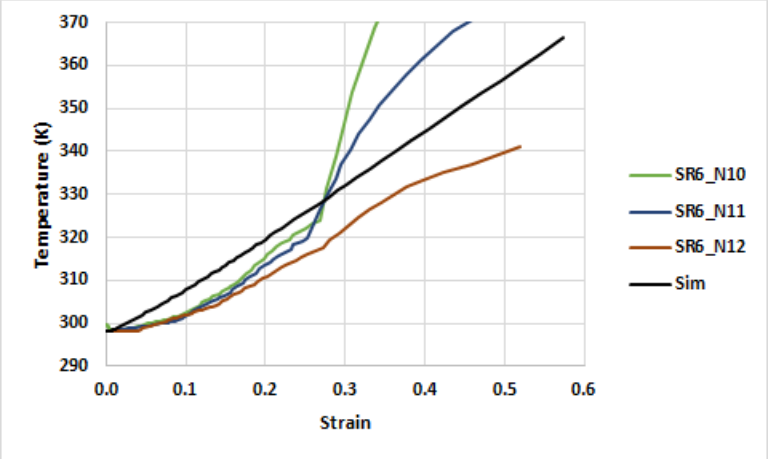

(b) temperature vs. strain

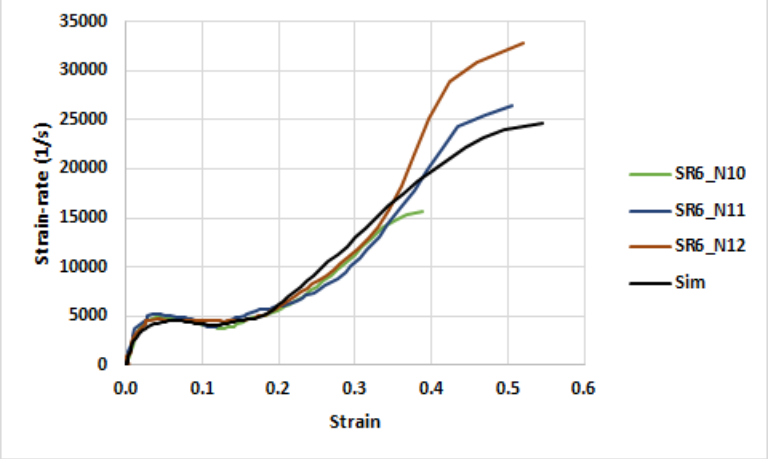

(c) strain rate vs. strain

Figure A-6. Comparison between tests and thermal-structural coupled simulations for Al2024 at the SR6 rate

B Ti64 tensile test simulation results in Step 1

Figure B-1. Comparison between tests and thermal-structural coupled simulations for Ti64 at the SR1 rate B-2
Figure B-2. Comparison between tests and thermal-structural coupled simulations for Ti64 at the SR2 rate B-3
Figure B-3. Comparison between tests and thermal-structural coupled simulations for Ti64 at the SR3 rate B-4
Figure B-4. Comparison between tests and thermal-structural coupled simulations for Ti64 at the SR4 rate B-5
Figure B-5. Comparison between tests and thermal-structural coupled simulations for Ti64 at the SR5 rate B-6

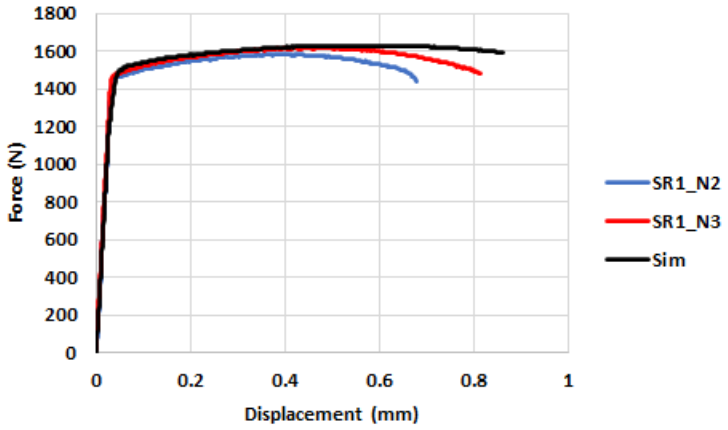

(a) force vs. displacement

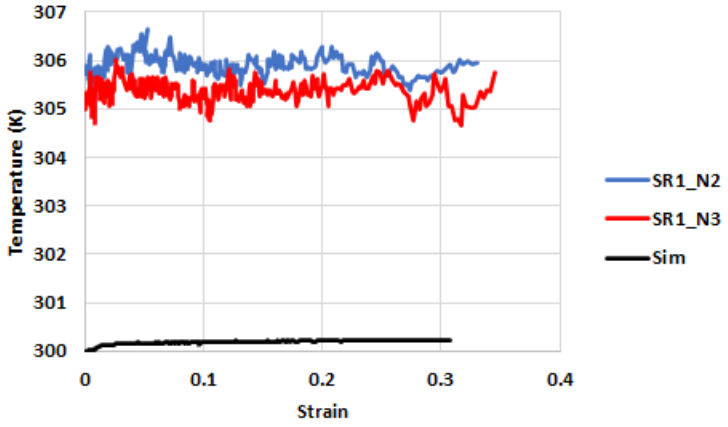

(b) temperature vs. strain

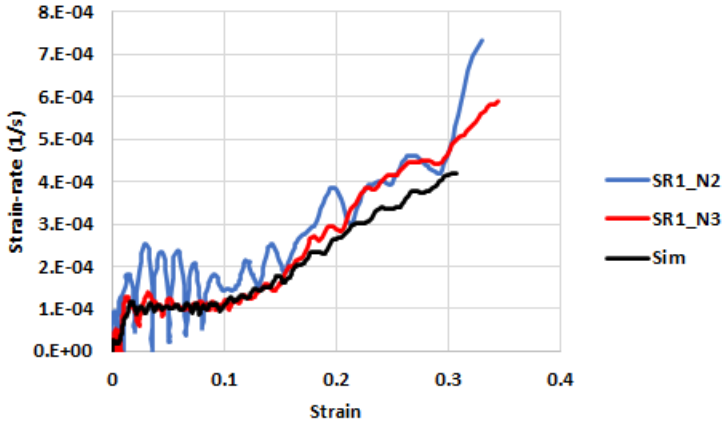

(c) strain rate vs. strain

Figure B-1. Comparison between tests and thermal-structural coupled simulations for Ti64 at the SR1 rate

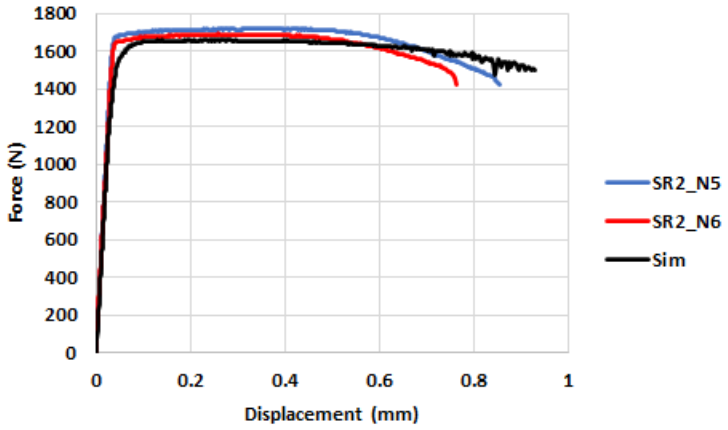

(a) force vs. displacement

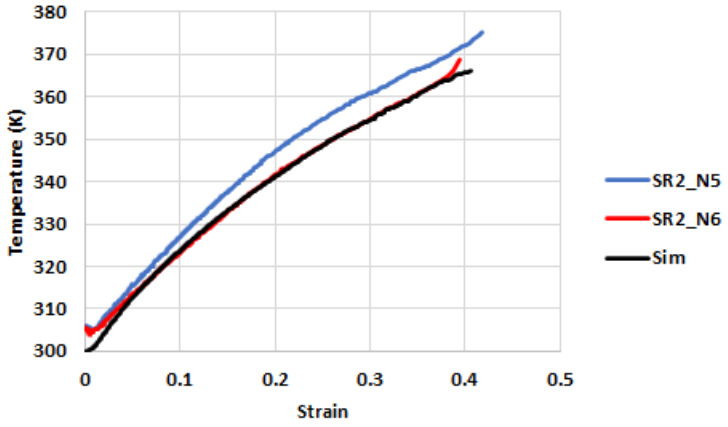

(b) temperature vs. strain

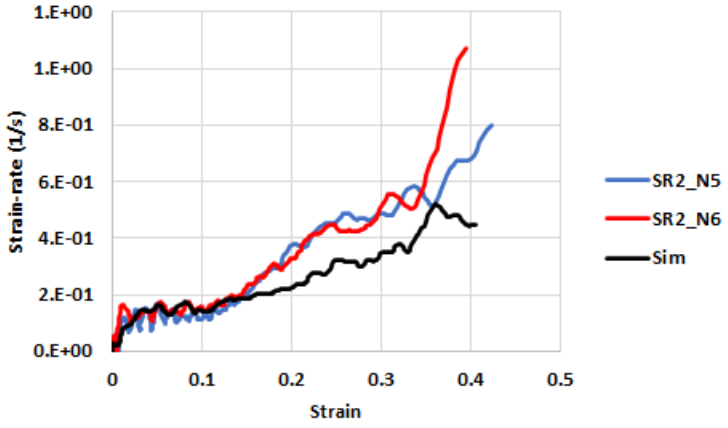

(c) strain rate vs. strain

Figure B-2. Comparison between tests and thermal-structural coupled simulations for Ti64 at the SR2 rate

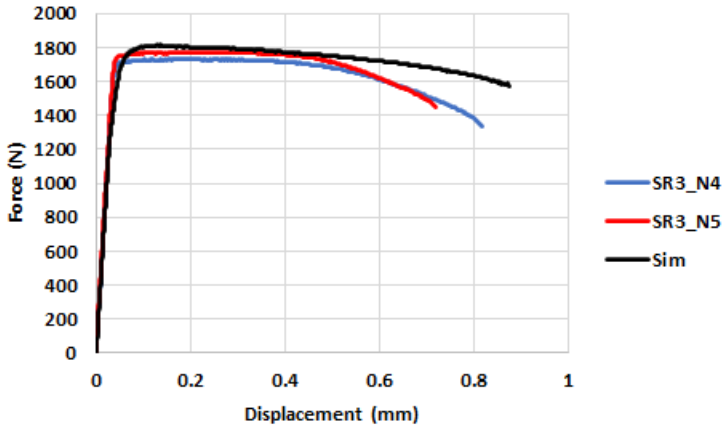

(a) force vs. displacement

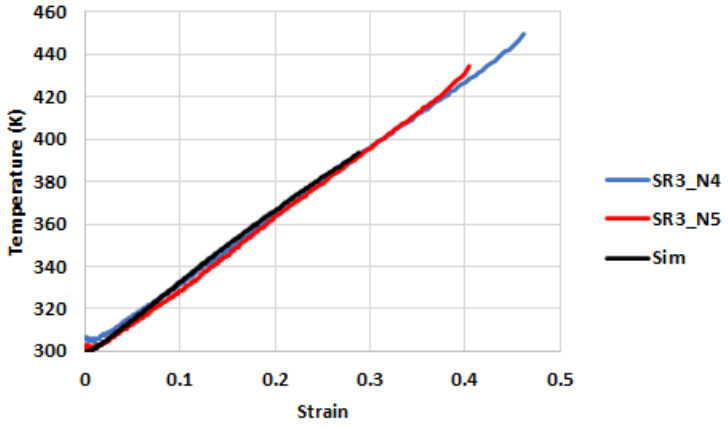

(b) temperature vs. strain

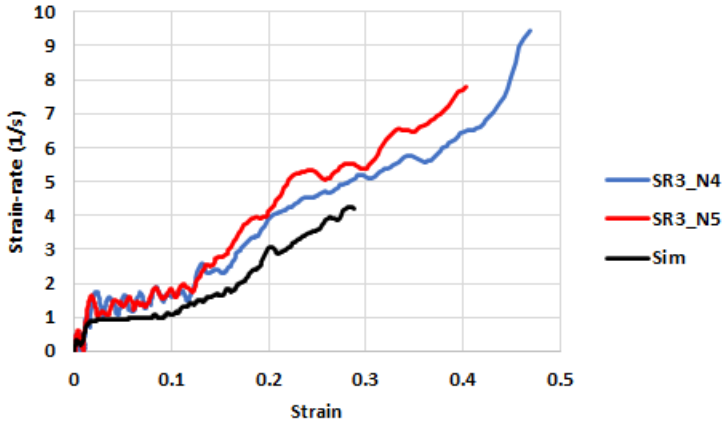

(c) strain rate vs. strain

Figure B-3. Comparison between tests and thermal-structural coupled simulations for Ti64 at the SR3 rate

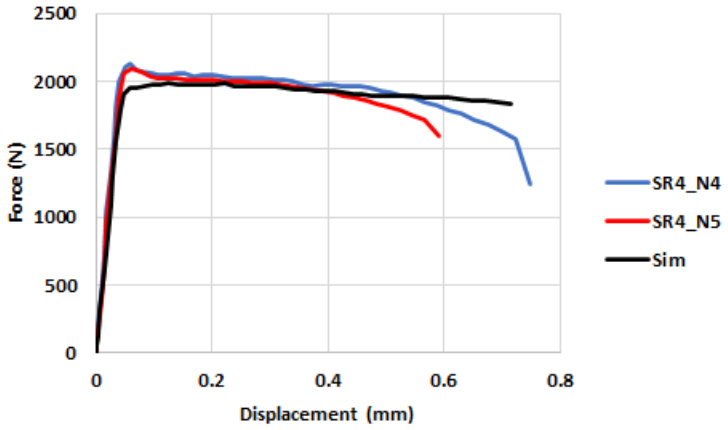

(a) force vs. displacement

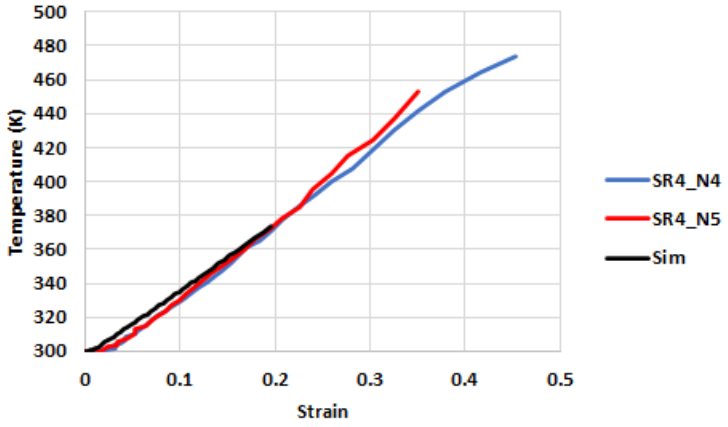

(b) temperature vs. strain

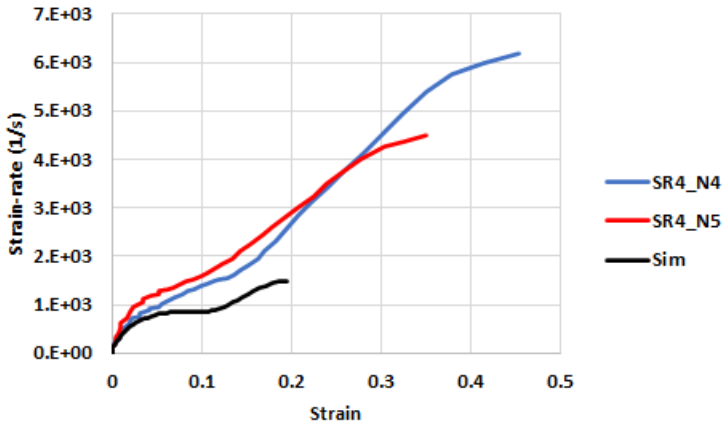

(c) strain rate vs. strain

Figure B-4. Comparison between tests and thermal-structural coupled simulations for Ti64 at the SR4 rate

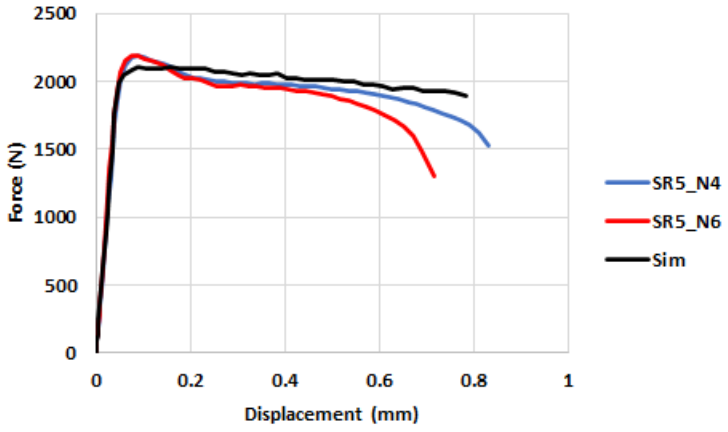

(a) force vs. displacement

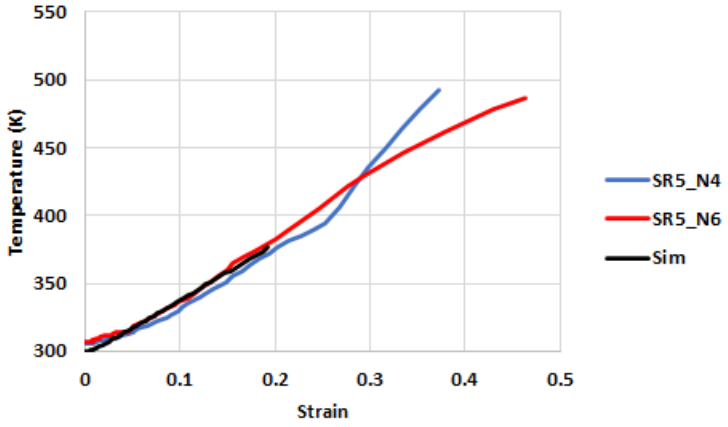

(b) temperature vs. strain

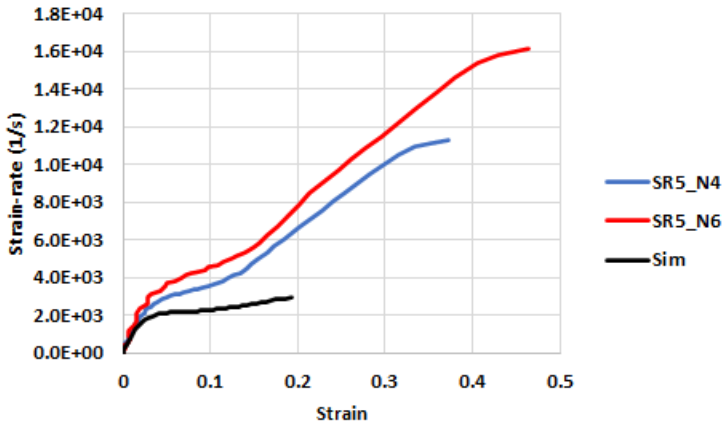

(c) strain rate vs. strain

Figure B-5. Comparison between tests and thermal-structural coupled simulations for Ti64 at the SR5 rate

C In718 tensile test simulation results in Step 1

Figure C-1. Comparison between tests and thermal-structural coupled simulations for In718 at the SR1 rate C-2
Figure C-2. Comparison between tests and thermal-structural coupled simulations for In718 at the SR2 rate C-3
Figure C-3. Comparison between tests and thermal-structural coupled simulations for In718 at the SR3 rate C-4
Figure C-4. Comparison between tests and thermal-structural coupled simulations for In718 at the SR4 rate C-5
Figure C-5. Comparison between tests and thermal-structural coupled simulations for In718 at the SR5 rate C-6

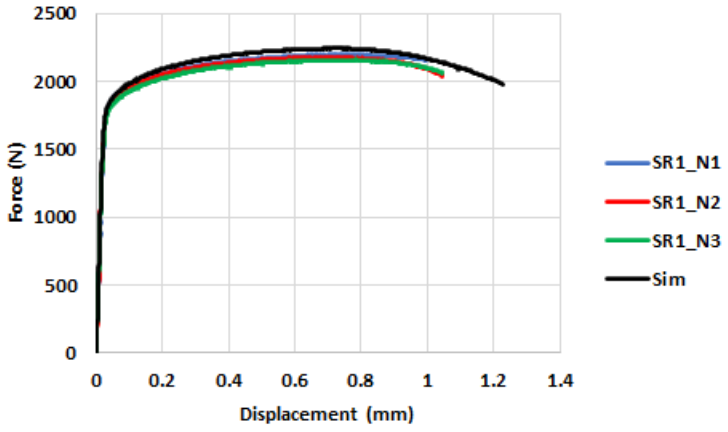

(a) force vs. displacement

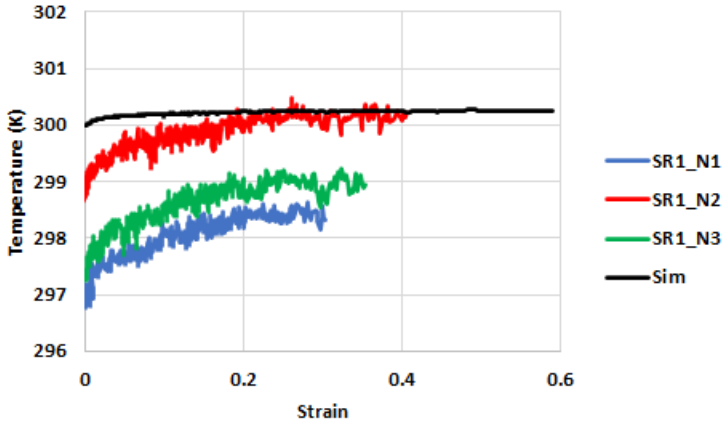

(b) temperature vs. strain

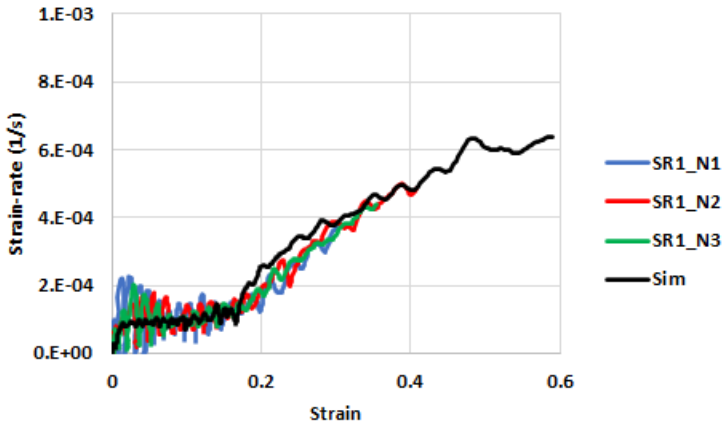

(c) strain rate vs. strain

Figure C-1. Comparison between tests and thermal-structural coupled simulations for In718 at the SR1 rate

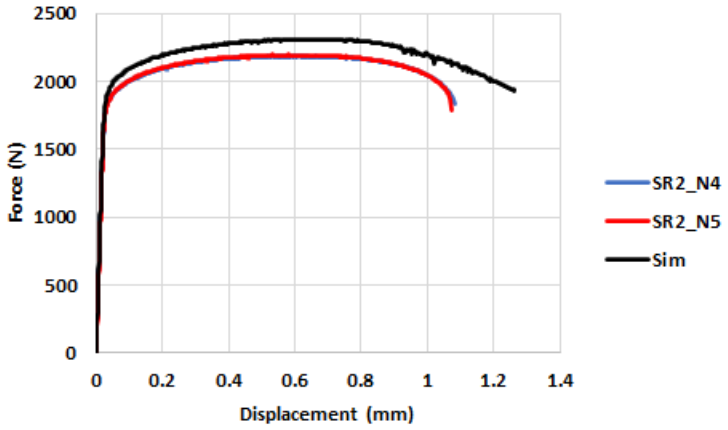

(a) force vs. displacement

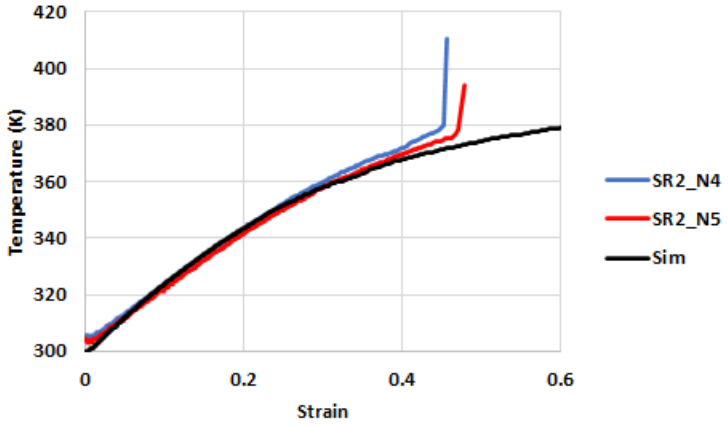

(b) temperature vs. strain

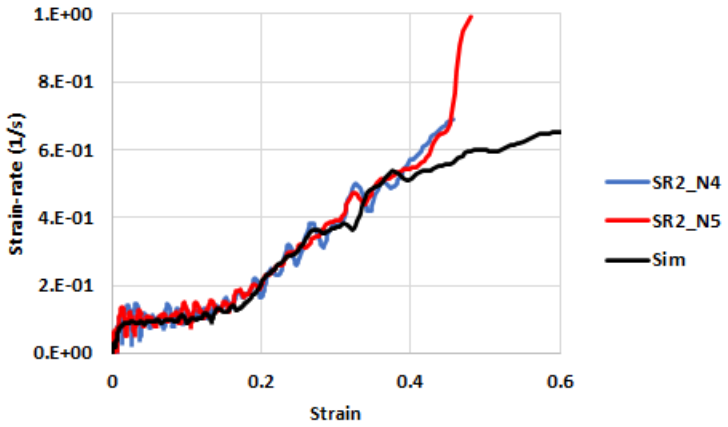

(c) strain rate vs. strain

Figure C-2. Comparison between tests and thermal-structural coupled simulations for In718 at the SR2 rate

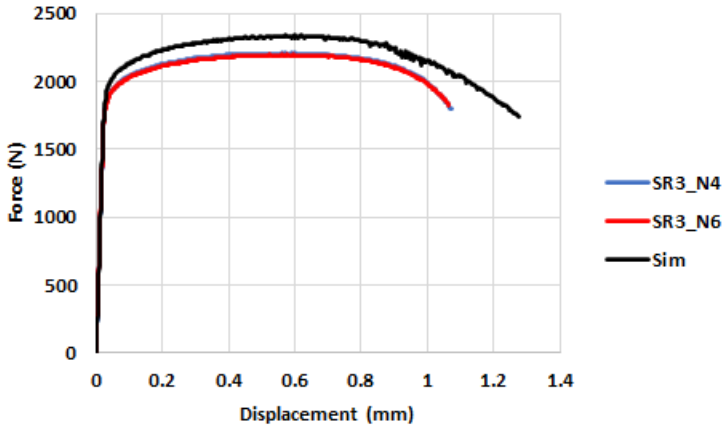

(a) force vs. displacement

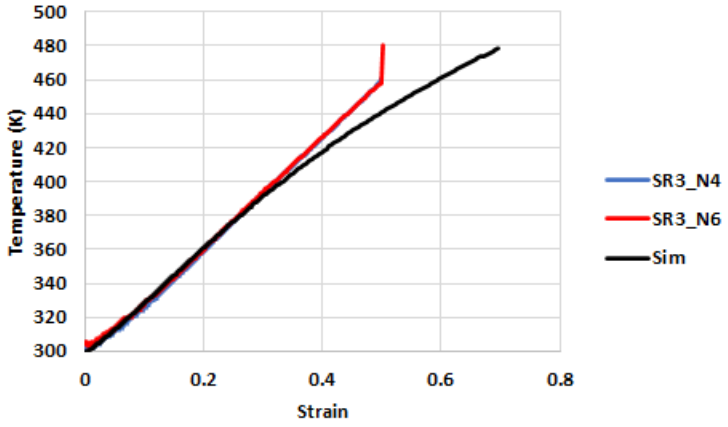

(b) temperature vs. strain

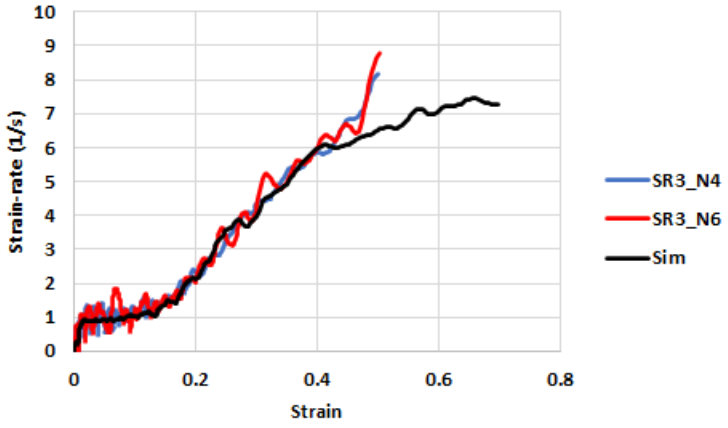

(c) strain rate vs. strain

Figure C-3. Comparison between tests and thermal-structural coupled simulations for In718 at the SR3 rate

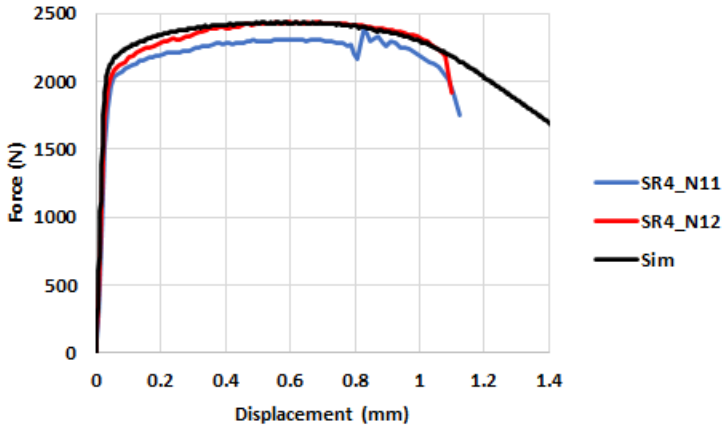

(a) force vs. displacement

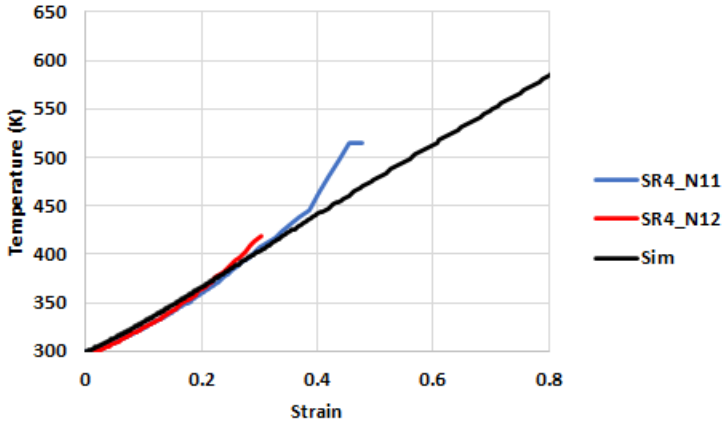

(b) temperature vs. strain

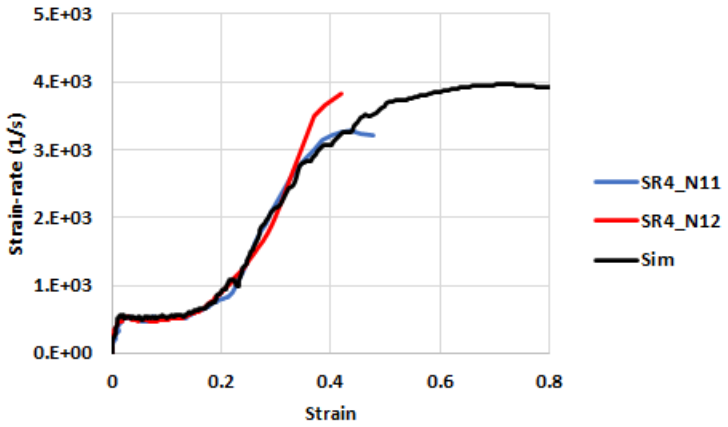

(c) strain rate vs. strain

Figure C-4. Comparison between tests and thermal-structural coupled simulations for In718 at the SR4 rate

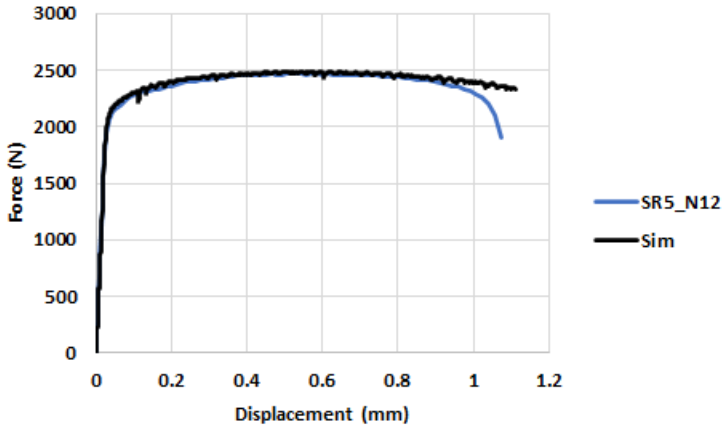

(a) force vs. displacement

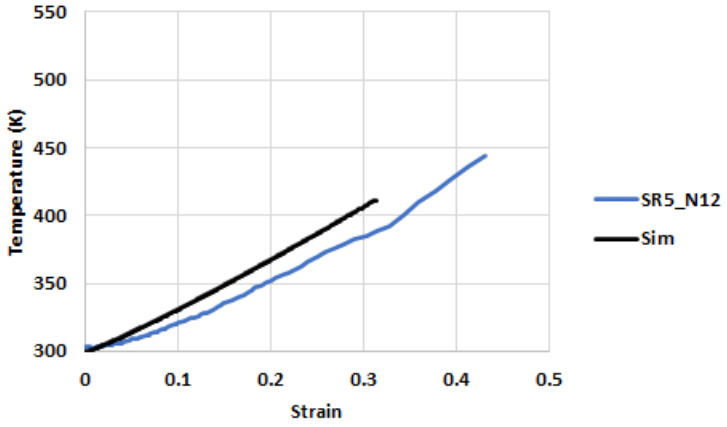

(b) temperature vs. strain

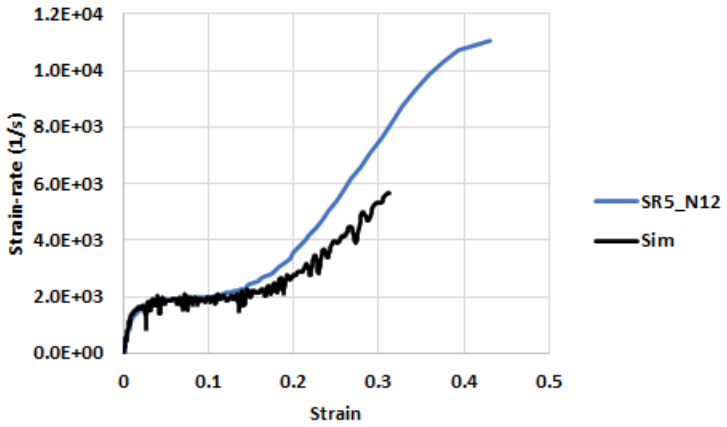

(c) strain rate vs. strain

Figure C-5. Comparison between tests and thermal-structural coupled simulations for In718 at the SR5 rate